NANO · MICRO small
www.small-journal.com

MXenes Antibacterial Properties and Applications: A Review and Perspective

Farzad Seidi, Ahmad Arabi Shamsabadi, Mostafa Dadashi Firouzjaei, Mark Elliott, Mohammad Reza Saeb, Yang Huang, Chengcheng Li, Huining Xiao, and Babak Anasori**

The mutations of bacteria due to the excessive use of antibiotics, and generation of antibiotic-resistant bacteria have made the development of new antibacterial compounds a necessity. MXenes have emerged as biocompatible transition metal carbide structures with extensive biomedical applications. This is related to the MXenes' unique combination of properties, including multifarious elemental compositions, 2D-layered structure, large surface area, abundant surface terminations, and excellent photothermal and photoelectronic properties. The focus of this review is the antibacterial application of MXenes, which has attracted the attention of researchers since 2016. A quick overview of the synthesis strategies of MXenes is provided and then summarizes the effect of various factors (including structural properties, optical properties, surface charges, flake size, and dispersibility) on the biocidal activity of MXenes. The main mechanisms for deactivating bacteria by MXenes are discussed in detail including rupturing of the bacterial membrane by sharp edges of MXenes nanoflakes, generating the reactive oxygen species (ROS), and photothermal deactivating of bacteria. Hybridization of MXenes with other organic and inorganic materials can result in materials with improved biocidal activities for different applications such as wound dressings and water purification. Finally, the challenges and perspectives of MXene nanomaterials as biocidal agents are presented.

1. Introduction

2D nanomaterials have found widespread applications in water treatment,[1] photocatalysis and electrocatalysis,[2–4] sensors,[5] and various biomedical purposes, including tissue engineering,[6,7] cancer therapy,[8,9] bio-imaging and antimicrobial applications.[10] One of the fast-growing areas of 2D materials is the MXenes family. MXenes are 2D transition metal carbides and nitrides with the general $M_{n+1}X_nT_x$ formula in which M stands for transition metal (such as Ti, V, Nb, and Mo), X represents carbon and/or nitrogen, n is 1–4, and T_x shows terminal groups of the MXenes (F, OH, O, etc.).[11–13] Various types of multilayered and delaminated MXenes have been synthesized and applied for different applications such as energy storage,[14] catalysis,[15] sensors,[16] separation,[17,18] and biomedical.[19] The fast growth of MXenes in different applications is due to their unique combination

F. Seidi, Y. Huang, C. Li
Jiangsu Co-Innovation Center of Efficient Processing and Utilization of Forest Resources and International Innovation Center for Forest Chemicals and Materials
Nanjing Forestry University
Nanjing 210037, P. R. China

A. Arabi Shamsabadi
Department of Chemistry
University of Pennsylvania
Philadelphia, PA 19104, USA

M. Dadashi Firouzjaei, B. Anasori
Department of Mechanical and Energy Engineering and Integrated Nanosystems Development Institute
Purdue School of Engineering and Technology
Indiana University–Purdue University Indianapolis
Indianapolis, IN 46202, USA
E-mail: banasori@iupui.edu

The ORCID identification number(s) for the author(s) of this article can be found under https://doi.org/10.1002/smll.202206716.

M. Dadashi Firouzjaei, M. Elliott
Department of Civil
Construction, and Environmental Engineering
University of Alabama
Tuscaloosa, AL 35487, USA

M. R. Saeb
Department of Polymer Technology
Faculty of Chemistry
Gdańsk University of Technology
G. Narutowicza, Gdańsk 11/12 80–233, Poland

H. Xiao
Department of Chemical Engineering
University of New Brunswick
Fredericton, New Brunswick E3B 5A3, Canada
E-mail: hxiao@unb.ca

B. Anasori
School of Materials Engineering
Purdue University
West Lafayette, IN 47907, USA

DOI: 10.1002/smll.202206716

of properties, including high hydrophilicity (water contact angles of 20–30° for $Ti_3C_2T_x$ and Ti_2CT_x films),[20] electronic conductivity (>20 000 S cm^{-1} for $Ti_3C_2T_x$ thin film),[21] and particular optical properties (a nonlinear absorption coefficient of -10^{-21} m^2 V^{-2} for $Ti_3C_2T_x$)[22] along with excellent ion adsorption capacity (a mercury ion adsorption capacity of 4806 mg g^{-1} for $Ti_3C_2T_x$ nanosheets).[23] Additionally, MXenes have the highest mechanical stiffness in solution-processed 2D materials at 300–400 GPa, for $Ti_3C_2T_x$ and $Nb_4C_3T_x$.[24]

MXenes have been widely employed for various types of biomedical applications such as biosensing, medicine, bioimaging, drug delivery, and cancer therapy. A combination of unique properties including rich chemistry, optical absorbance, metallic conductivity, redox trait, excellent electron transfer capability along with high hydrophilicity, and acceptable biocompatibility are unique features of MXenes for the development of biosensors for in vitro and in vivo analyses.[25] For instance, the changes in the surface terminations of MXenes through interactions with different molecules (such as various redox agents) lead to significant variations in MXenes properties.[26,27] The pH- and near-infrared (NIR)-responsive behavior makes them suitable candidates for fabrication of controllable MXene-based drug delivery systems.[28,29] Moreover, MXenes can eradicate tumor cells by synergistic photothermal ablation and chemotherapy due to their high photo-to-heat conversion efficacy.[30] Among various biomedical applications of MXenes, their antimicrobial uses have attracted increasing attention and are the main focus of this review. Microbial infection is still a serious issue worldwide, causing millions of deaths annually. While various antibiotics have been developed to defeat bacterial infections, the overuse of antibiotics resulted in the mutation of bacteria and the generation of antibiotic-resistance versions that are challenging to be treated with the present antibiotics. Therefore, the production of new generations of antibiotics is vital. One strategy to deal with this issue is using various antibacterial nanomaterials such as carbon nanotubes (CNTs),[31] graphene-based nanomaterials,[32–34] metal-organic frameworks (MOFs),[35,36] metal nanoparticles,[37] polymeric nanoparticles,[38] and metal oxide nanoparticles.[39,40] MXenes are among the newest candidates for antimicrobial nanomaterials.

A major advantage of MXenes over many other nanomaterials is the tunability of their atomic structure and composition to provide more vigorous antimicrobial activities as we cover in this review. Additionally, MXenes can be processed in different forms, such as thin films[41,42] or thick membranes,[43–45] and can be combined with polymers to fabricate polymer composites.[46] Since most MXene compositions are composed of C, N, and nontoxic transition metals (Ti, Nb, Ta) to biological tissues, they have shown good biocompatibility as they can be degraded and disposed in the body of mice.[47,48] Therefore, antibacterial MXenes are proper candidates to be used for treating infected wounds without any concerns about cell cytotoxicity. In this review, first, we provide a brief discussion about the MXene structure types, compositions and their synthesis, and other critical properties for antibacterial applications. We then present the possible antibacterial modes of action of MXenes, followed by recent progress in the fabrication and development of antibacterial MXenes along with various structural factors that can affect the biocidal activity of MXene nanosheets. Additionally, we discuss various types of modifications to improve the biocidal performance of MXenes and summarize the applications of MXenes as biocompatible biocidal agents at the end of this review.

2. Synthesis of MXenes

MXenes are mainly synthesized via top-down chemical etching routes and most precursors used to date are MAX phases. The $M_{n+1}AX_n$, generally known as MAX phases, are hexagonal close-packed nanolayered compounds of ternary transition metal carbides and nitrides.[49–51] M is an early transition metal (Ti, Nb, V, etc.), A refers to an element mainly from IIIA and IVA groups in the periodic table (such as Al and Si), X represents C, N, or a mixture of them, and n can be 1–4.[52] There are four main types of MAX phase structures named 211, 312, 413, and 514 representing M_2AX, M_3AX_2, M_4AX_3, and M_5AX_4, respectively. The main difference between these MAX phase structures is the number of MX layers between each A layer (**Figure 1**).

Up to now, synthesis of over 155 MAX phases have been reported.[51] The M, A, and X elements that have been used in MAX phases are illustrated in Figure 1 and marked in blue, red, and black colors. MAX phases have several unique properties in the world of ceramics as they are machinable and thermal shock resistant and thermally/electrically conductive. However, MAX phase layers have weak biocidal activities, whereas 2D MXenes are well-known for excellent biocidal activities through various mechanisms discussed later in this review.

Different methods for the synthesis of MXenes are summarized in **Figure 2**. Selective etching is a top-down chemical procedure for fabricating MXenes from the MAX phase through selective removal of the A layer. Up to now various etchant methods have been practiced for this goal including hydrofluoric acid (HF) etching,[12] acid/fluoride salt etching (such as hydrochloric acid (HCl)/sodium fluoride (NaF),[59] HCl/lithium fluoride (LiF),[60] HCl/iron trifluoride (FeF_3),[61] and ammonium hydrogen difluoride ($(NH_4)HF_2$[62]), alkali etching,[63,64] electrochemical etching,[65,66] and molten salt etching.[13,67] Different etching agents can strongly affect the type and content of the terminal groups of MXenes nanosheets, flake size, and morphology, which can possibly impact the antimicrobial activities of MXenes. However, the effect of this factor has not been studied yet.

Among all these methods, utilizing an aqueous HF solution for selective etching of the A layer in MAX phases has been widely explored.[12] Typically, the etching process using a HF solution to synthesize $Ti_3C_2T_x$ from Ti_3AlC_2 MAX phase involves the removal of the Al layer in the form of AlF_3 to produce the multilayered $Ti_3C_2T_x$ MXene with OH, O, and F terminal groups. Subsequent delamination through chemical intercalation or mechanical exfoliation of the HF-etched-MXenes produces the monolayer delaminated $Ti_3C_2T_x$ nanosheets. Usually, chemical intercalation delamination with cations such as Li ion has been used as the method to weaken the dominant interlayer forces, and then MXene nanosheets are produced by a mild manual shaking or sonication.[68] Multilayered MXenes have been intercalated by various organic molecules

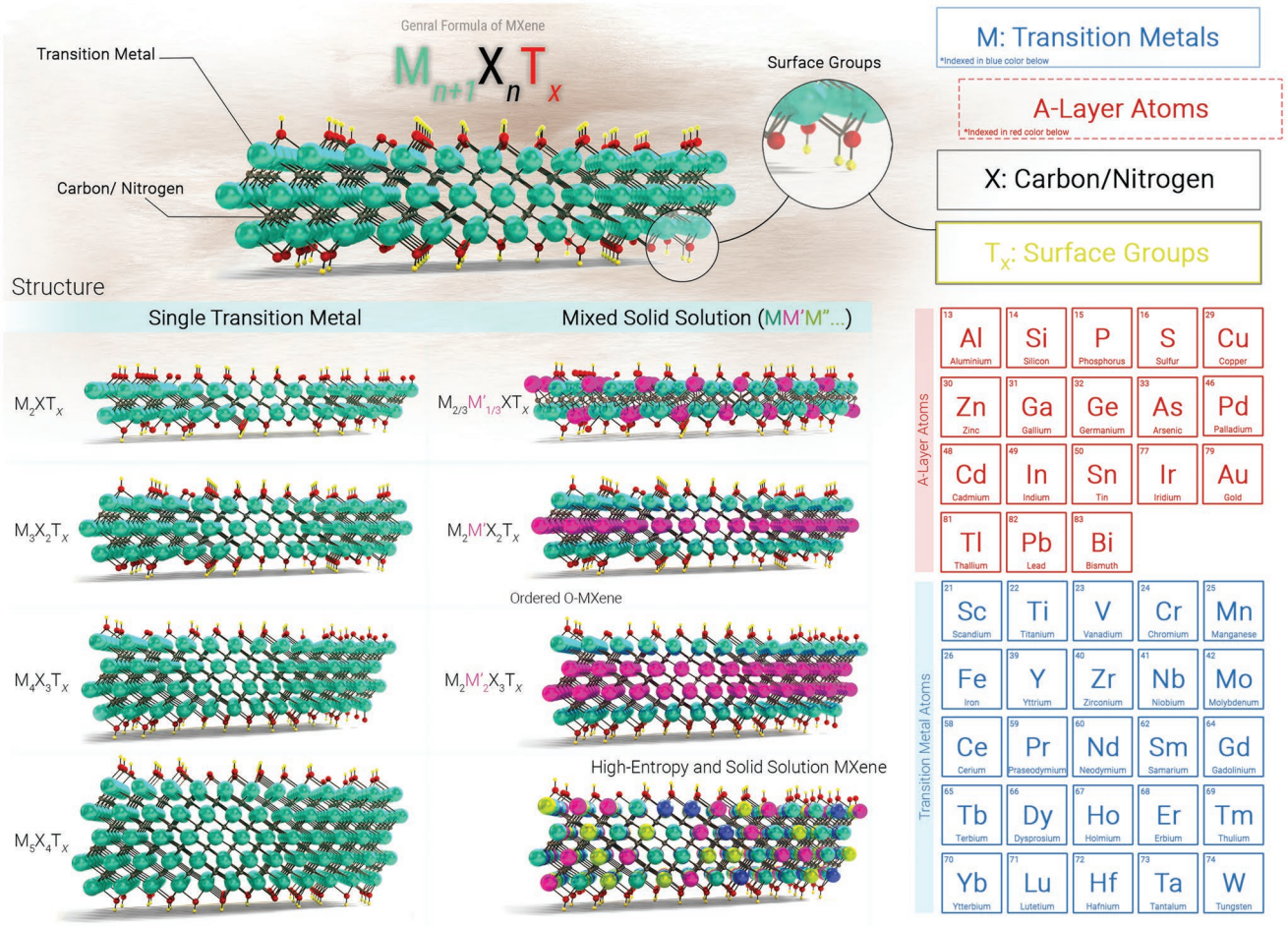

Figure 1. Different structures of MXenes and the possible elements that have been utilized for the fabrication of different MAX phases.

(such as hydrazine,[69] dimethyl sulfoxide (DMSO),[69] urea,[69] *n*,*n*-dimethylformamide,[69] isopropylamine,[70] and *n*-butylamine[71]), surfactants [72] and cations.[73,74] More recently, three-roll milling was shown to be an effective method of mechanical exfoliation without the need for any cation intercalants.[75]

Chemical transformations, including ammoniation of transition of metal carbides,[54] carburization of transition metal sulfides,[55] and deoxygenation and carburization,[56] are other top-down methods for MXenes synthesis. Chemical vapor deposition (CVD)[57] and salt-templated growth[58] are bottom-up methods for synthesizing high-quality thin sheets of MXenes. CVD affords MXenes with high purity and fewer defects, unlike the etching method. However, fabrication of monolayer MXenes by CVD has not been achieved yet, implying the requirement for further development and modification of this procedure. To the best of our knowledge, the antibacterial activity of the MXenes prepared by these bottom-up methods has not been explored.

3. Critical Properties of MXenes for Antibacterial Applications

This section covers the most critical properties of MXenes that can contribute to their antibacterial activities. The properties of MXenes depend on the composition, layer number, and size of the nanosheets. These properties can determine the applications of MXenes in various fields, including as antimicrobial agents.

3.1. Effect of Structural Properties of MXene on Their Antibacterial Properties

MXenes have 2D hexagonal close-packed structures in which M elements are in a closely packed configuration, and X atoms are positioned in the octahedral sites. The terminal functional groups (T) on the surface of MXenes are usually −OH, =O, or −F, as discussed earlier.[76–78] MXene 2D layers are connected through weak van der Waals and H-bonding interactions of the surface termination groups. However, the M-X and M-T atoms in interlayers are bonded by strong covalent and ionic bonds. A layer of $Ti_3C_2T_x$ as the most utilized MXene has a thickness of ~ one nanometer as it was measured using atomic force microscopy (AFM).[79–81] When MXene flakes are stacked in the form of films or composite structures, the distance between two MXenes nanosheets (interlayer distance) can vary depending on the intercalant species in between layers, and it is usually around <1.0 to 1.5 nm in MXene films.

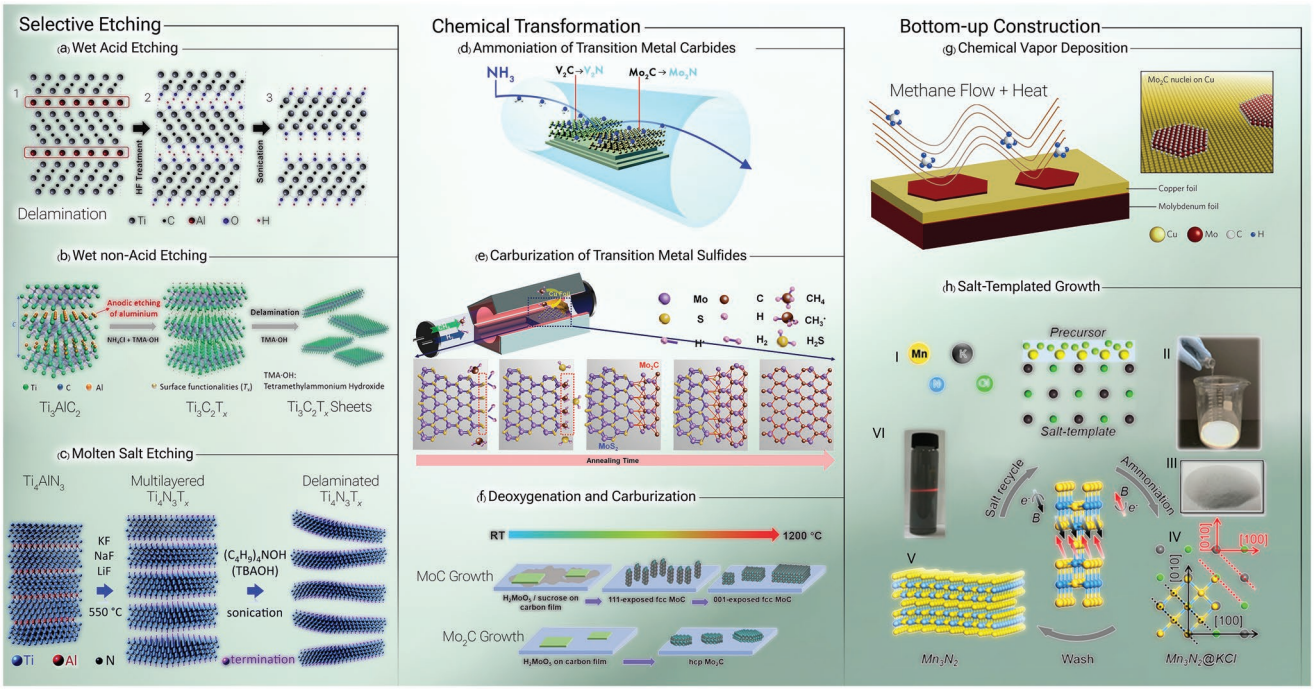

Figure 2. Different MXenes synthesis approaches.[12,13,53–58] I) Top-down methods: a) A Ti_3AlC_2 exfoliation procedure via wet acid etching MAX/non-MAX phases; b) wet etching MAX phase without acid; and c) fabrication of multilayered and delaminated $Ti_4N_3T_x$ via molten salts at 550 °C under argon atmosphere. II) Chemical transformation approaches. d) Ammoniation of V_2C and Mo_2C to obtain their transition metal nitrides V_2N and Mo_2N at high temperatures; e) carburization of MoS_2 to Mo_2C under H_2 and CH_4; and f) synthesized Mo_2C MXene by carburization and de-oxygenation of MoC. III) Bottom-up methods. g) Chemical vapor deposition (CVD) of α-Mo_2C on a Cu support; and h) salt-templated growth procedure to prepare Mn_3N_3 MXene under an ammonia atmosphere.

The delamination and intercalation conditions of MXenes can impact their biocidal activity.[82] Sonication in different solvents, such as water, DMSO, and isopropylamine, and in the presence of different compounds, such as hydrazine monohydrate, NaOH, and KOH leads to MXene nanosheets with different physiochemical properties (**Table 1**). Evaluation of the antibacterial activity against *Escherichia coli* (*E. coli*) using the colony forming unit (CFU) count method showed that the required time for inactivating 50% of bacteria by 100 µg mL^{-1} multilayer $Ti_3C_2T_x$ was ≈280 min which was reduced to 137, 120, 76, 53, 80, and 70 min, respectively, for MXenes sonicated in water, DMSO, isopropylamine, hydrazine monohydrate, NaOH, and KOH.[82] The more robust antibacterial activity of isopropylamine- and hydrazine monohydrate-treated MXenes were attributed to the more oxidative severe damage to cell membranes by generating higher contents of the reactive oxygen species (ROS).

Beyond the surface of MXenes, the morphology and the core M-X atomic structures of MXenes can change their bactericidal properties.[83] When multilayer MXene powders are delaminated (increase of the sonication time in **Figure 3**a–c), larger inhibition zones were observed due to the more accessible sharp edges in delaminated MXenes for two Nb_2CT_x and $Nb_4C_3T_x$ MXenes. By increasing the sonication time for the delamination of MXenes, the lateral flake sizes are reduced (Figure 3b,c left to right panels), which leads to more effective-

Table 1. Physiochemical properties of different $Ti_3C_2T_x$ MXenes treated with different delamination and intercalation agents.[82]

Treatment	d-space [Å]	Thinness [nm]	Zeta Potential [mV]	Hydrodynamic Diameter [nm]
Untreated	9.8	N/A	−20.5	N/A
Water delamination	10.2	284	−23.2	1003
DMSO delamination	10.6	30	−17.8	783
iPA delamination	12.9	24	−16.5	288
HMH intercalation	13.2	14	−27.1	341
NaOH intercalation	12.1	11	−23.4	262
KOH intercalation	12.2	10	−24.3	215

Abbreviations: iPA = isopropylamine; HMH = hydrazine monohydrate.

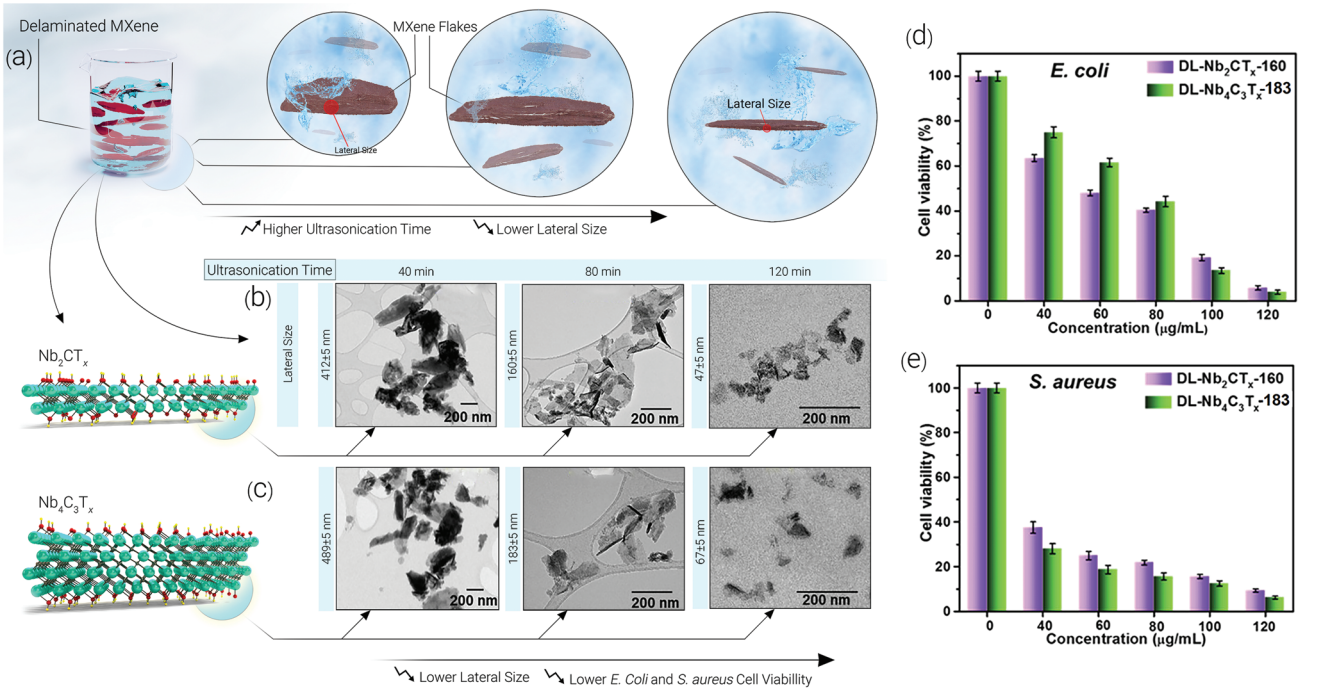

Figure 3. a) Schematic illustration of different MXene flakes with various lateral sizes. It has been shown that increasing the ultrasonication time would decrease the lateral size of the MXene flake. Chemical structure and TEM images of b) Nb_2CT_x and c) $Nb_4C_3T_x$ MXene nanosheets were delaminated by ultrasonication after 40, 80, and 120 min. Increasing concentrations of both MXenes to 120 μg mL^{-1} would decrease the cell viability of d) *E. coli* and e) *S. aureus* treated with delaminated $Nb_4C_3T_x$ and Nb_2CT_x. Adapted with permission.[83] Copyright 2020, American Chemical Society.

ness of MXenes toward killing the *E. coli* and *Staphylococcus aureus* (*S. aureus*). Also, increasing concentrations of both MXenes to 120 μg mL^{-1} would decrease the cell viability of *E. coli*, and *S. aureus* treated with delaminated $Nb_4C_3T_x$ and Nb_2CT_x ((Figure 3d,e). Additionally, the thickness of the MXene core (n in $M_{n+1}X_nT_x$) can affect the antimicrobial performance of MXenes. For example, while Nb_2CT_x and $Nb_4C_3T_x$ have similar M-X bonds (Nb-C), the former has two layers of M with a layer of X (Nb-C-Nb), and the latter has four layers of M atoms, and three layers of X atoms (Nb-C-Nb-C-Nb-C-Nb). The bactericidal activity of the thicker MXene, that is $Nb_4C_3T_x$, is slightly lower than the thinner MXene (Nb_2CT_x) as shown in Figure 3. These studies indicate that the number of layers can play a critical role in the ultimate antimicrobial behavior of MXenes.

Besides the morphology of MXene layers, the types and contents of the surface terminations (T) can also affect the properties of MXenes.[84,85] Hydroxyl (−OH) and fluoride (−F) groups require one electron to reach a stable state, whereas oxygen (=O) needs two electrons to attain a stable state. It has been reported that =O terminations provide higher strength and better thermodynamic stability than the other termination groups.[86–88] By increasing temperature and longer storage, the OH-terminated surfaces tend to be converted into O-terminated surfaces by releasing H_2 gas. To the best of our knowledge, the effect of the surface functional groups of MXenes on their antimicrobial behavior has not been determined. Comparative studies with other similar nanomaterials highlighted the critical role of the surface functional groups in the biocidal activity of the nanomaterials.[89,90]

3.2. Effect of Optical Properties of MXene on Their Antibacterial Properties

MXenes have tunable optical properties depending on their composition and structure[91] and can strongly absorb lights in a wide range from ultraviolet-visible (UV–Vis) to NIR areas,[92] which leads to their biomedical applications in photoacoustic imaging (PAI) and photothermal therapy (PTT).[93–96] In addition to the strong absorption in the solar spectrum, high surface area and abundant free radical distribution can contribute to the photo-to-thermal conversion of MXenes. They can absorb light energy significantly owing to their satisfactory electromagnetic wave absorption capacity. Also, a high density of the surface carriers of MXenes can produce heat, and thereby dominates their photothermal activities. The photothermal of MXenes adds fast light-to-heat conversion to the inherent antibacterial blade effect and could boost the final antibacterial activity through the so-called *nanothermal blade* effect (**Figure 4**a). Through the production of heat, PTT is able to enhance the permeability of bacterial membranes and increase the intracellular penetration of ROS and metal ions. Additionally, hyperthermia from light-to-heat conversion in PTT leads to protein denaturation and damage to DNA in the bacteria structure.[97,98] Notably, resistance to PTT, despite resistance to antibiotics, is a less likely phenomenon.[99] The UV-Vis-NIR spectra of MXenes have been used as a guide for photothermal conversion. The absorption spectrum of $Ti_3C_2T_x$ in the range of 400–1200 nm showed a broad peak at 650–850 nm; thus, $Ti_3C_2T_x$ can absorb light at 808 nm, and this phenomenon can add rapid temperature increase and lead to improved biocidal

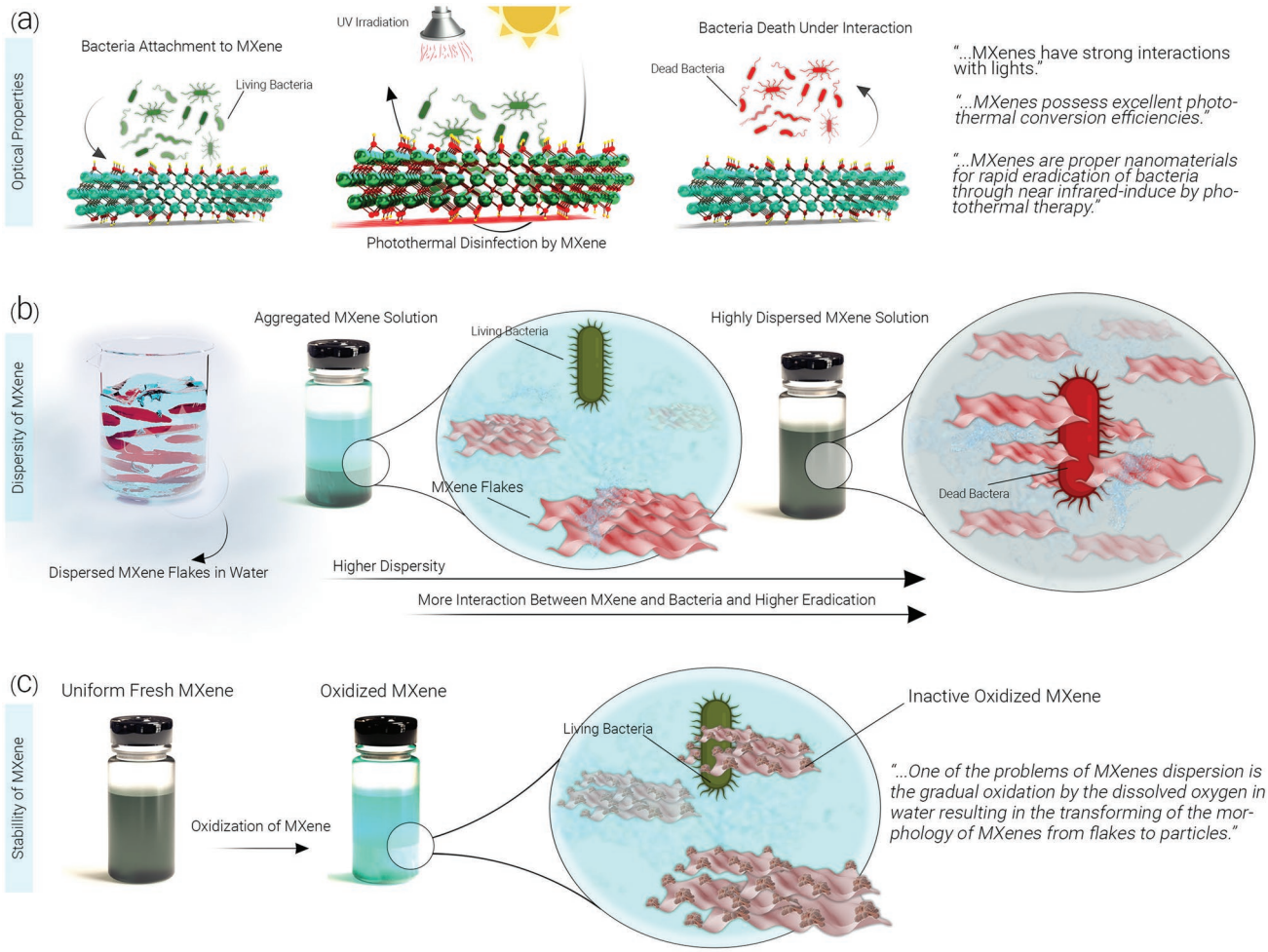

Figure 4. The effect of a) optical properties, b) dispersity, and c) stability of MXene on their antibacterial properties. MXenes' high photothermal conversion efficiency would enforce a high near infrared-induced effect that would inhibit the bacteria cell by photothermal therapy. The high dispersity of nanomaterials in water would increase the active surface area for interaction with bacteria. Therefore, higher biocidal rates can be obtained; however, the oxidation of MXene would negatively affect this parameter.

activity. In contrast, lights with wavelengths out of this range (e.g., 532 and > 980 nm) on $Ti_3C_2T_x$ has almost no light-to-heat effects. Nb_2CT_x has a broad peak in the NIR with a maximum peak at ≈915 nm[91] and had been used in photothermal studies in NIR-I (750–1000 nm) and NIR-II (1000–1350 nm).[93] The photothermal effect of $Ti_3C_2T_x$ nanosheets has an internal light-to-heat conversion efficiency of 100%, indicating a perfect energy conversion.[95] The MXene-coated polyvinylidene fluoride (PVDF) could absorb the sunlight and increase the temperature to 75 °C in <400 s. Additionally, light absorption can induce the generation of singlet oxygen ($^1O_2$) on the surface of MXene nanosheets.[100,101]

MXenes effective photothermal properties can be used for rapidly eradicating bacteria through NIR-induced PTT.[102,103] The temperature of colloidal dispersions of $Ti_3C_2T_x$ at concentrations of 30, 250, and 500 µg mL^{-1} upon 5 min irradiation at 808 nm increased to around 45, 55, and 65 °C, respectively, indicating the significant photothermal effect of $Ti_3C_2T_x$ nanosheets.[103] Additionally, the excellent biocompatibility of the highly concentrated MXene suspension (500 µg mL^{-1}) can be attributed to replacing the fluorine terminal groups with -OH groups through hydrothermal treatment MXenes under exposure to a NaOH solution.[103] Upon 20 min of NIR irradiation at 808 nm on 100 µg mL^{-1} of $Ti_3C_2T_x$ solution, effective bacterial inhibition (>95% of *E. coli* & >99% *S. aureus*) was achieved.[102] Further investigations proved the ability of $Ti_3C_2T_x$/NIR for fast eradication of other 13 types of gram (–) and (+) bacteria, even antibiotic-resistant bacteria such as vancomycin-resistant enterococcus (VRE).[102] Unlike $Ti_3C_2T_x$, Nb_2CT_x showed weak biocidal activity even in the light, and V_2CT_x/NIR showed vigorous biocidal activity only against *S. aureus*. The reason is attributed to the strong plasmonic properties of $Ti_3C_2T_x$.[104] Indeed, a plasmonic peak in the range of 650–850 nm in the NIR region was reported for $Ti_3C_2T_x$ which 808 nm light is within this range. However, no peak was observed in that region for Nb_2CT_x and V_2CT_x.

The photothermal conversion effect provided by MoO_{3-x}QDs/$Ti_3C_2T_x$ on fabrics inhibits bacterial growth.[105] The presence of $Ti_3C_2T_x$ endows excellent biocidal activity against *E. Coli* and *S. aureus* under light with a very high sterilization rate of

99%. ROS are generated because of the electronic transition of MoO_{3-x}QDs/$Ti_3C_2T_x$. After passing through the cell membranes, the reaction of the generated ROS with organic substances in the bacteria leads to bacteria death. Generally, the excellent antibacterial performance of the MXene-based composites can be ascribed to high electrical conductivity, promotion of carbon layers, and high photothermal conversion effect. These properties endow MXenes' capability for killing bacteria through synergistic heat generation and oxidative stress. It has been reported that nanomaterials with photothermal[106,107] and oxidative stress[108,109] properties are proper candidates for antimicrobial applications. Figure 4a graphically summarizes the effect of MXenes' optical properties on their antibacterial properties.

3.3. Effect of MXenes Dispersion on Their Antibacterial Properties

Under the dispersed condition, the stability of the dispersion has a great influence on the antimicrobial properties of the system. Aggregation and sedimentation reduce the contact area between the bacteria with the antibacterial agent whose ultimate effect is the decline in the antibacterial properties. Addition of chelating ligands is a common strategy for improving the stability of colloids[110] and has been developed for stabilization of MXenes colloids.[111,112] Practically, MXenes dispersions have high colloidal stability in water due to their highly hydrophilic surface. The negative effect of agglomeration on the antimicrobial activity of CNTs and graphene-based nanomaterials was reported previously.[33,113] For example, the presence of high content of oxygen groups on graphene oxide (GO) endows higher dispersibility for GO compared to reduced GO (rGO). Higher dispersibility, in turn, provides more opportunities for GO to be in contact with bacteria and deactivate bacteria through sharp edges.[114] The comparison of the antibacterial activity of different graphene-based nanomaterials against *E. coli* showed the strong effect of the degree of dispersibility on the biocidal activities so that the order of GO > rGO > graphite (Gt) > graphite oxide (GtO) was reported for the antibacterial activities.[115] In the case of MXenes, agglomeration in aqueous colloidal solutions is a less likely phenomenon. Mahmoud et al. reported a higher antibacterial activity for the delaminated-$Ti_3C_2T_x$ dispersion compared to that of the multilayered-$Ti_3C_2T_x$ dispersion.[116,117] At concentration of 100 μg mL^{-1}, the delaminated-$Ti_3C_2T_x$ showed antibacterial efficacy of 97.7 and 97.0% against *E. coli* and *B. subtilis* whereas these values were 30.6 and 33.6%, respectively, for the multilayered-$Ti_3C_2T_x$. Less agglomeration tendency in the delaminated-$Ti_3C_2T_x$ along with a higher number of sharper edges provide more contact with the cell membrane, in comparison to the multilayered-$Ti_3C_2T_x$, resulting a stronger antibacterial activity for the delaminated-$Ti_3C_2T_x$.

Due to the −F, −OH, and =O termination groups, MXenes have negative zeta potentials in −30 to −60 mV under neutral conditions.[118] The high surface charge of MXenes combined with their high hydrophilicity allows high dispersion of MXene nanosheets in water through H-bonding formation between H_2O and the terminal groups.[118,119] Comparison of the colloidal dispersibility of delaminated $Ti_3C_2T_x$ flakes modified with hydrazine and KOH, and with water as the control showed improved dispersibility of KOH- and hydrazine-modified $Ti_3C_2T_x$ samples.[120] The pH of aqueous solutions of hydrazine-$Ti_3C_2T_x$, KOH-$Ti_3C_2T_x$, and control $Ti_3C_2T_x$ were around 7.8, 9.8, and 6.5, respectively, indicating a higher number of terminals –OH groups in the modified ones. The dispersion of these MXenes remained almost stable at pH values of 5–12 without agglomeration whereas at pH< 5, closer to the isoelectric points can lead to lower electrostatic repulsion and reduced dispersibility. Accordingly, the MXenes can produce stable dispersions under physiological pH conditions without any surfactant.

The stable colloids of MXenes in various solvents allow the fabrication of membranes through vacuum filtration, spin- and spray-coating methods for developing thin-films,[121,122] and uniform composites by mixing with other materials.[123,124] So far, the influence of MXenes dispersity on their antibacterial properties is unknown. Determining the relationship between MXenes' dispersity and their biocidal activity is critical for antibacterial and biological applications. Figure 4b graphically summarizes the effect of MXenes' dispersity on their antibacterial properties.

3.4. Effect of MXene Stability on Their Antibacterial Properties

One of the main shortcomings of MXenes' dispersion is the gradual degradation by hydrolysis in water and the dissolved oxygen in solutions, transforming the morphology of MXenes from flakes to oxide particles.[125–127] Metal oxide nanoparticles show fewer sharp edges than nanoflakes which can decline the antibacterial activity of MXenes. Therefore, removal of the dissolved oxygen in water by degassing[128] or adding antioxidant agents such as sodium ascorbate[129] to suppress the oxidation of MXenes during the storage period can prevent such a devastating phenomenon. Modification of MXenes can also improve the stability against oxidation.[120] However, controlled oxidation of MXene flakes can be beneficial for their antibacterial performance, by formation of anatase TiO_2 nanocrystals on amorphous carbon through controlled oxidation of $Ti_3C_2T_x$ in air.[130] Aging $Ti_3C_2T_x$ membrane for 30 days improved its antibacterial performance. While the fresh $Ti_3C_2T_x$ membrane impeded the growth of *E. coli* and *Bacillus subtilis (B. subtilis)* by 67 and 73%, respectively, the 30-day aged membrane hindered the growth of 99% of both *E. coli* and *B. subtilis* colonies.[131] The formation of TiO_2 nanocrystals on the membrane surface due to $Ti_3C_2T_x$ degradation is beneficial for improving the overall antibacterial properties. Figure 4c graphically summarizes the effect of MXenes' stability on their antibacterial properties. Generally, modification of MXene surface with antibacterial agents can protect MXenes from oxidation and might have a dual effect on the MXenes stability and antibacterial activity.

3.5. Effect of MXene Flake Size on Their Antibacterial Properties

The size and shape of 2D nanomaterials are critical factors in determining the ultimate biocidal activity.[132,133] The size of

nanosheets directly affects dispersibility, adsorption ability, and the number of sharp edges that can physically damage the microorganisms' membrane. Incubation of *E. coli* with 100 μg mL^{-1} $Ti_3C_2T_x$ nanosheets with lateral sizes 0.09, 0.35, 0.57, and 4.40 μm for 3 h under dark conditions reduced the bacteria viability by 70, 55, 40, and 20%, respectively and the values for *B. subtilis* were around 92, 90, 85 and 75%, respectively.[134] These results indicate the binding effect of the size of nanosheets. Smaller MXenes flakes exposed more sharp edges and a higher possibility for diffusion into the cells to damage the cytoplasmic components, including DNA.

Using Nb-based MXenes, Pandey et al. showed that the size of nanosheets of MXenes could change their bactericidal properties.[83] Increasing the time of sonication for delamination delivers nanosheets with smaller sizes. For both $Nb_4C_3T_x$ and Nb_2CT_x, the antibacterial activity of MXenes against *E. coli* and *S. aureus* increased for MXenes with smaller lateral sheet sizes due to the sharper edges and more corners in smaller nanosheets. Scanning electron microscopy (SEM) images (**Figure 5**) clearly showed the membrane damage with cell lysis induced by the MXene nanosheets.

3.6. Effect of MXene Surface Charges on Their Antibacterial Properties

Generally, positively-charged nanomaterials can adsorb bacteria species because bacteria have a net negative surface charge under most environmental conditions. In nanomaterials with negative surface charges, surface modification has been used to enhance their anchoring activity. For example, the GO nanosheets were modified using azithromycin, citraconic anhydride (CA), and polyethyleneimine to prepare nanocomposites with a positive surface charge.[135] Selective anchoring of bacteria, induced by the positive surface charge and destructive effect of GO,[136] results in bacteria death.

$Ti_3C_2T_x$ colloidal solutions with low concentrations have shown weak biocidal activity. This observation can be related to the negative surface charge of both MXene and bacteria, which minimizes their contact in dilute solutions. The tunable chemistry of MXenes allows for adjusting their surface charge through functionalization.[137] Using cationic polymeric poly-L-lysine (PLL) molecules, the surface charge of delaminated $Ti_3C_2T_x$ flakes was changed toward a positive value.[138] Compared to the pristine $Ti_3C_2T_x$ with a negative surface charge, electrostatic adsorption of *E. coli* with the modified surface charge engineering MXene (positively charged) reduces the number of viable cells by two orders of magnitude at 200 mg L^{-1}.

Phage therapy using a bacteriophage is an effective method to combat bacteria species. However, bacteria species alter during a bacteriophage's attack by preventing adsorption of the bacteriophage and inhibiting bacteriophage DNA entry. To combine bacteriophage target properties and the antibacterial potential of MXene, bacteriophages were bonded to $Ti_3C_2T_x$ nanofragments.[139] To attach bacteriophages to MXene, it was modified by Fe ions to prepare MXene with the Fe–O functional group, followed by mixing the freeze-dried modified MXene with the bacteriophage suspension. Electrostatic interactions between MXene and bacteriophage result in the formation of a potent antibacterial agent. Besides targeting bacteria by a bacteriophage, ROS and sharp edges of MXenes cause membrane rupture (**Figure 6**). High accumulation of MXene in the bacteriophage cell wall enhances its attachment to the bacteria membranes, leading to the fast killing of bacteria.

Molecular dynamics (MD) simulation of interactions between highly positivity-charged modified $Ti_3C_2T_x$ MXene nanosheets with a model bacterial membrane showed that adsorbed MXene on the membrane surface promoted a local phase transition in a domain wherein the fluidity of the phospholipid was similar to that of the gel phase.[140] The lipids directly under the MXene adhered to the MXene surface and showed different collateral translation motions from the surrounding phospholipids. The

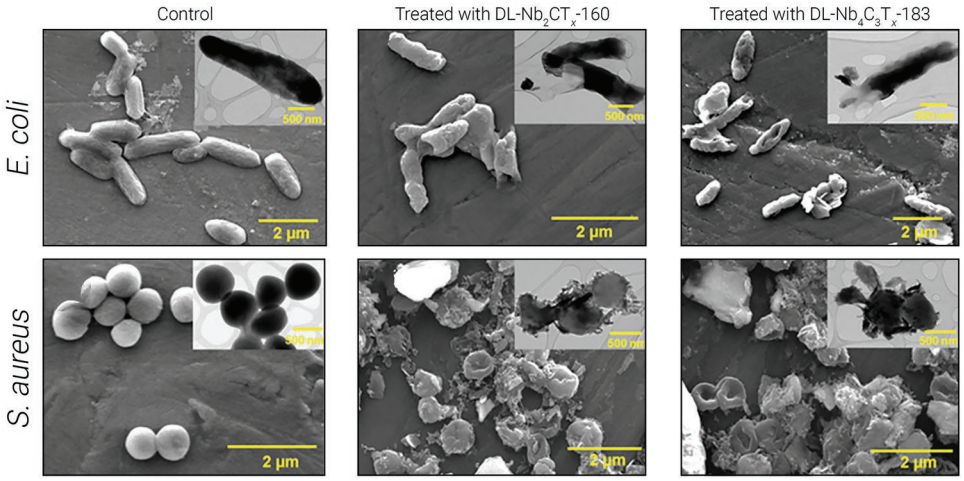

Figure 5. SEM images of bacteria cells (a) before treating, and after treating with 120 μg mL^{-1} of, b) delaminated- Nb_2CT_x nanosheets with lateral sizes of 160 nm (delaminated-Nb_2CT_x-160) and c) delaminated-$Nb_4C_3T_x$ with lateral sizes of 183 nm (delaminated-$Nb_4C_3T_x$-183). Adapted with permission.[83] Copyright 2020, American Chemical Society.

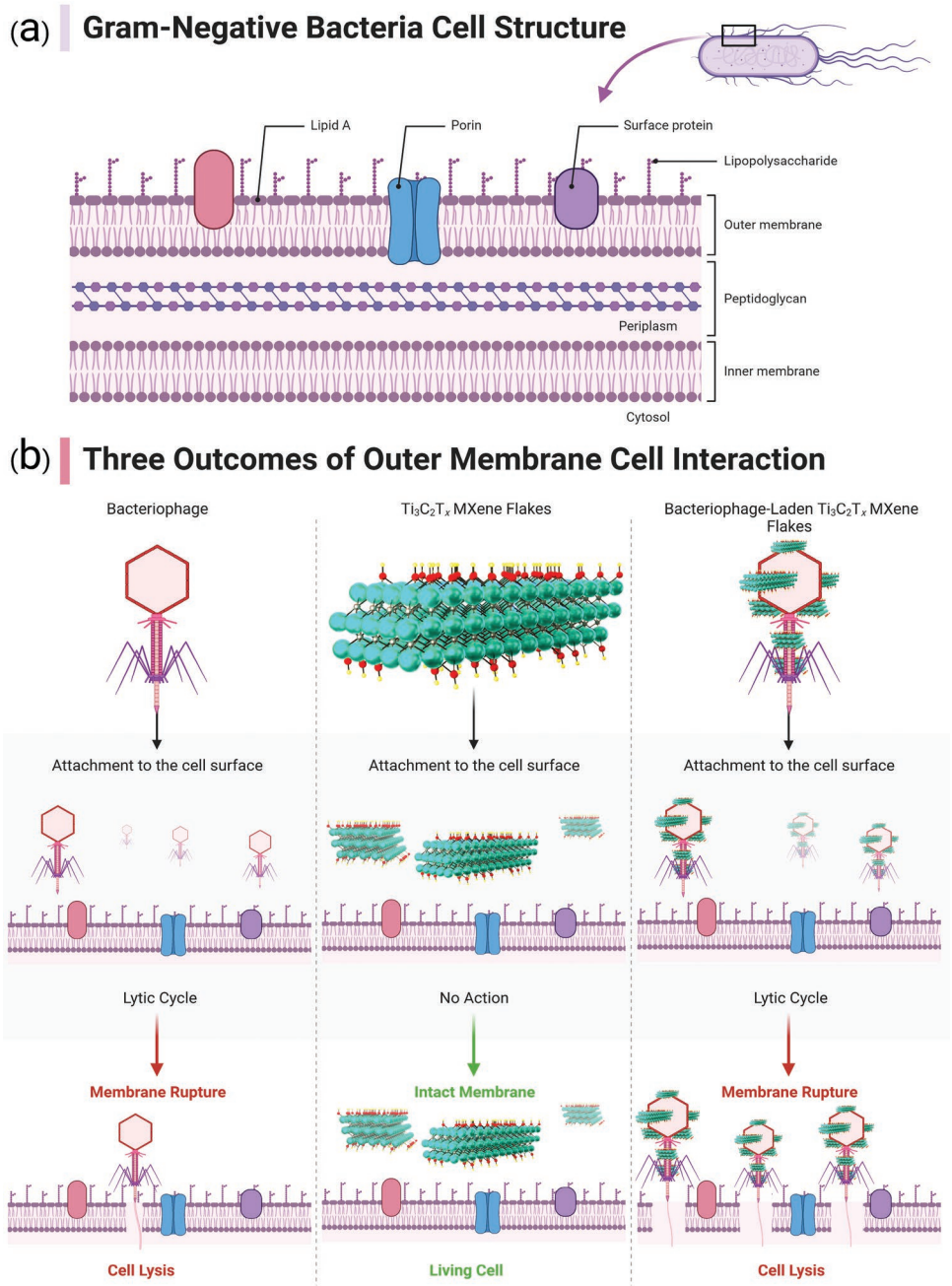

Figure 6. a) The schematic illustration of gram-negative bacteria cell structure. b) Three outcomes of out membrane cell interaction with bacteriophage, $Ti_3C_2T_x$ MXene, and bacteriophage-laden $Ti_3C_2T_x$ MXene.[139]

strong electrostatic interactions between the highly-charged MXene surface and zwitterionic lipid head groups lead to the formation of a denser and thinner phospholipid membrane in the MXene-phospholipids layer domain compared to the peripheral phospholipids. As a result, it impacts the lateral diffusion of the bacterial phospholipids layer. The tension between the two phases results in defect formation in the membrane, reducing its resistance and ultimately leading to cell death due to the leakage of molecules from the phase boundary defects caused by the adsorbed MXene nanosheets.

4. MXenes as Antimicrobial Agents

4.1. Antimicrobial Modes of Action

Before presenting different MXenes antibacterial behavior and effectiveness, we summarized various modes of action against different microorganisms investigated and proposed (**Figure 7**). Because study of the antimicrobial activity of MXenes is still in its infancy, more investigations on the antimicrobial mechanisms and mode of action of these 2D nanomaterials are required.

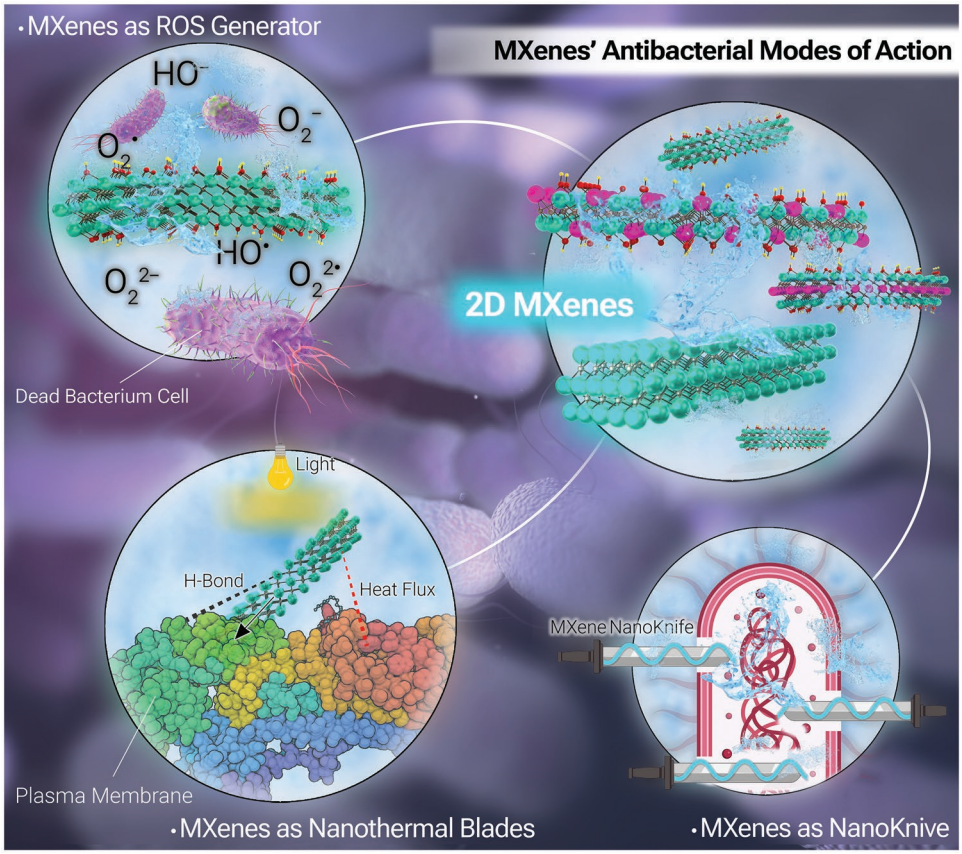

Figure 7. Antibacterial mechanisms of MXenes.

4.1.1. MXenes as NanoKnives

The first study on the antibacterial activity of MXenes by Rasool et al. proposed the damage to the cell walls of bacteria by the sharp edges (the so-called "nanoknives") of 2D $Ti_3C_2T_x$ nanosheets,[141] which is similar to the proposed antibacterial mechanisms for GO or rGO through the mechanical damage of cell membranes.[115,132,142,143] SEM images of bacteria after interaction with MXene flakes showed severe membrane disruption and cytoplasm leakage induced by the sharp edges of $Ti_3C_2T_x$ nanosheets (**Figure 8**a). By increasing the MXene concentration, the bacteria are trapped or wrapped with thin sheets of MXene and then form agglomerates. In addition to the sharp edges, other factors were essential for the antibacterial activity of $Ti_3C_2T_x$, including 1) high hydrophilicity and anionic nature of $Ti_3C_2T_x$ enhance the bacteria inactivation via direct the contact-killing mechanism; 2) H-bonding between oxygenate groups of MXene with lipopolysaccharide cords on the bacteria membrane disrupts the nutrient intake by the bacteria.

The detailed study on the antibacterial mechanism of colloidal $Ti_3C_2T_x$ nanosheets by Shamsabadi et al. confirmed the damage to the cell wall by the sharp edges of MXenes.[134] Incubation of *E. coli* and *B. subtilis* with 100 µg mL^{-1} $Ti_3C_2T_x$ nanosheets with a relatively small lateral size (90 nm) for 3 h under dark conditions reduced the bacteria population by 70 and 92%, respectively. As can be seen, a higher activity against Gram-positive bacteria was observed for $Ti_3C_2T_X$ compared to Gram-positive bacteria and it agrees well with previous studies.[141,144] The difference in antibacterial activity of MXene toward both bacteria species might be related to dissimilarities in the structure and surface charge of the bacteria. The outer protective lipid membrane in the cell wall of Gram-negative bacteria can prevent direct damage of MXene nanoknives.[141] Despite a thick peptidoglycan layer in the cell wall of Gram-positive bacteria, the deficiency of the protective membrane makes them vulnerable upon exposure to the sharp flakes of MXene. In addition, as $Ti_3C_2T_X$ is negatively charged more repulsion may be created with Gram-negative bacteria as they have lower isoelectric points than those of Gram-positive bacteria. Same behavior was observed for GO and GO-Ag-MOF nanomaterials.[34]

By increasing the contact time to 8 h, the antibacterial effect of 90-nm MXene was increased to >95% against both bacteria species. The proposed mode of action involved a first direct contact of MXene nanosheets with the bacteria surface and then tearing down the bacteria wall by the sharp edges of the MXenes (Figure 8b). Bacterium's cell wall which has a thickness of around 20–50 nm[145,146] can be cut easily by the sharp edges of MXenes (1 nm). It was speculated that smaller nanosheets permeate the microorganisms through direct physical penetration or endocytosis. The penetrated nanosheets cleave the DNA of bacteria leading to their death (Figure 8b).

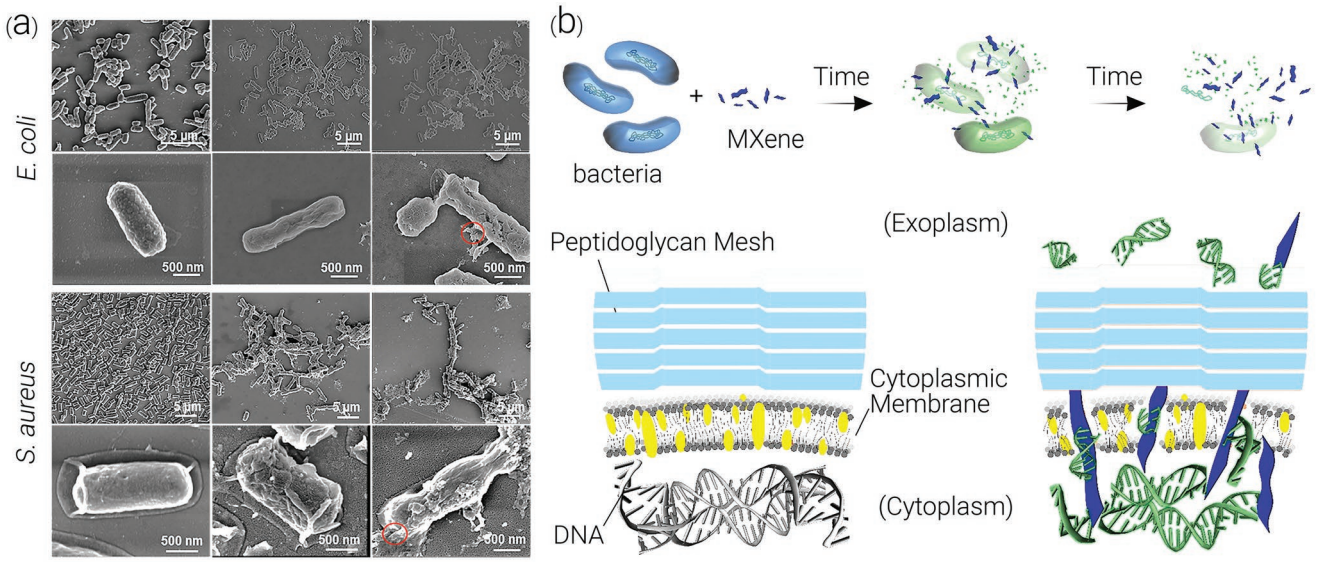

Figure 8. a) SEM images of the *E. coli* and *B. subtilis* after treating, respectively, with A) 0 μg mL^{-1}, B) 50 μg mL^{-1}, and C) 100 μg mL^{-1} $Ti_3C_2T_x$. The cell membrane remained intact in the absence of MXene, whereas membrane disruption cytoplasm leakage (see red circles) was observed in MXene. Adapted with permission.[141] Copyright 2015, American Chemical Society. b) The schematic proposed mechanism for the antimicrobial property of $Ti_3C_2T_x$ nanosheets. Adapted with permission.[134] Copyright 2018, American Chemical Society.

4.1.2. MXenes as ROS Generators

The so-called ROS are chemically reactive oxygen molecules with unpaired electrons that have the ability to kill bacteria and cancer cells.[147] Four main types of ROS are superoxide anion radicals ($O_2^{\bullet-}$), hydrogen peroxide (H_2O_2), singlet oxygen ($^1O_2$), and hydroxyl radicals ($^{\bullet}OH$). These reactive oxygens are produced either from water or oxygen through a series of complex redox reactions. In most of the studies, the activation energy for these reactions is provided by the absorption of light. Ultrasound has also been used as an alternative strategy for generation of ROS by MXenes even under dark conditions. ROS generation by MXenes through ultrasound has mainly been applied for cancer treatments.[148–152] However, to the best of our knowledge, the responses of MXenes to ultrasound for antibacterial applications are not investigated yet. In the process of ROS generation, the oxidation of water sequentially produces hydroxyl radicals, hydrogen peroxide, superoxide anion radicals, and singlet oxygen whereas incomplete reduction of oxygen can sequentially produce superoxide anion radicals, hydrogen peroxide, and hydroxyl radicals.[153,154]

ROS generation and oxidative stress production have been proven for most of the well-known 2D nanomaterials.[155,156] Due to the rich electronic properties of MXenes,[101,157] oxidative stress and generation of ROS have been considered as other pathways for killing bacteria in MXenes.[83] It has been shown that active Ti-O sites on the surface of $Ti_3C_2T_x$ nanosheets can form electron/hole pairs upon light irradiation. The available surface terminal groups and excellent electrical conductivity of MXenes prevent the electron/hole re-combinations, and thereby boost the photocatalytic activity. The redox reactions on the surface of MXenes induce ROS generation; therefore, the generated ROS by a few-layer $Ti_3C_2T_x$ is much higher compared to that of multilayer $Ti_3C_2T_x$ nanosheets.[158,159] In fact, the ROS generation in MXenes is related to their intrinsic structure and electronic properties. Therefore, various factors such as the number of MX layers, stacking of the MXene sheets and their sizes, defects, and doping can modulate the ROS generation of MXenes. Additionally, density functional theory (DFT) calculations have shown that the surface terminations and surface modification of MXenes can significantly change the optical, mechanical, and electrical properties of MXenes which directly can affect the redox capability and ROS generation by MXenes.[157,160]

$Ti_3C_2T_x$ nanosheets with fewer stacked sheets produce higher ROS content due to the higher content of available Ti-O surfaces, which leads to more redox reaction sites.[159] The steady-state concentrations of different ROS types by $Ti_3C_2T_x$ flakes intercalated by different agents in the presence of UV or vis light are given in **Table 2**.[120] The presence of light was essential as very low ROS can be produced in dark conditions. This result clearly shows the effect of the intercalation of MXenes on their ROS generation capability (**Figure 9**a). Additionally, these data suggest the photochemical stability in hydrazine-$Ti_3C_2T_x$ > KOH-$Ti_3C_2T_x$ > water-$Ti_3C_2T_x$. Indeed, surface-adsorbed K^+ in KOH-$Ti_3C_2T_x$ generates a middle layer that hinders coupling between Ti^{3+} and ROS. In contrast, chemically adsorbed hydrazine molecules to the surface of hydrazine-$Ti_3C_2T_x$ flakes provide stability by absorbing photoelectrons and reacting with the generated ROS.

ROS are produced and consumed by different microorganisms at controlled concentrations; however, excess ROS induces oxidative damage to biomacromolecules (such as lipids, proteins, and DNA) and cell membranes in microorganisms, which can lead to mitochondrial dysfunction and cell death. The effect of MXene type and dose on the intracellular ROS level in *E. coli* (Figure 9b) indicates inhibiting the activity of antioxidant enzymes in bacteria by MXenes, which results in accumulation

Table 2. The steady-state concentrations of different ROS types produced by different intercalated $Ti_3C_2T_x$ flakes under UV-Vis illumination after 24 h (HMH = hydrazine).[120]

	MXene	$^1O_2$[$\times 10^{-14}$ mol L^{-1}]	$^{\bullet}OH$ [$\times 10^{-15}$ mol L^{-1}]	O_2^- [$\times 10^{-9}$ mol L^{-1}]
UV	H_2O-$Ti_3C_2T_x$	6.23	4.17	6.28
	HMH-$Ti_3C_2T_x$	0.83	1.21	1.05
	KOH-$Ti_3C_2T_x$	1.63	2.38	2.56
Vis	H_2O-$Ti_3C_2T_x$	3.47	2.82	3.96
	HMH-$Ti_3C_2T_x$	0.83	0.94	0.83
	KOH-$Ti_3C_2T_x$	1.20	1.52	2.10

of ROS inside the cells.[82] The excess ROS induces oxidative damage to various cell segments. Levels of protein oxidation in *E. coli* incubated with different concentrations of $Ti_3C_2T_x$ confirmed the higher oxidation levels at higher MXene concentrations (Figure 9c). Additionally, high malondialdehyde production, a product of membrane lipid peroxidation, confirms the oxidative damage to the bacteria membrane by ROS generation from MXenes (Figure 9d). The decline in superoxide dismutase activity, an essential antioxidant enzyme in bacteria, upon incubation with MXenes (Figure 9e) indicates the deactivating of this enzyme by ROS generation.

4.1.3. MXenes as Nanothermal Blades

MXenes have excellent photothermal activity,[100,161] and therefore, killing bacteria through the photothermal process upon light irradiation has been considered one of the mechanisms

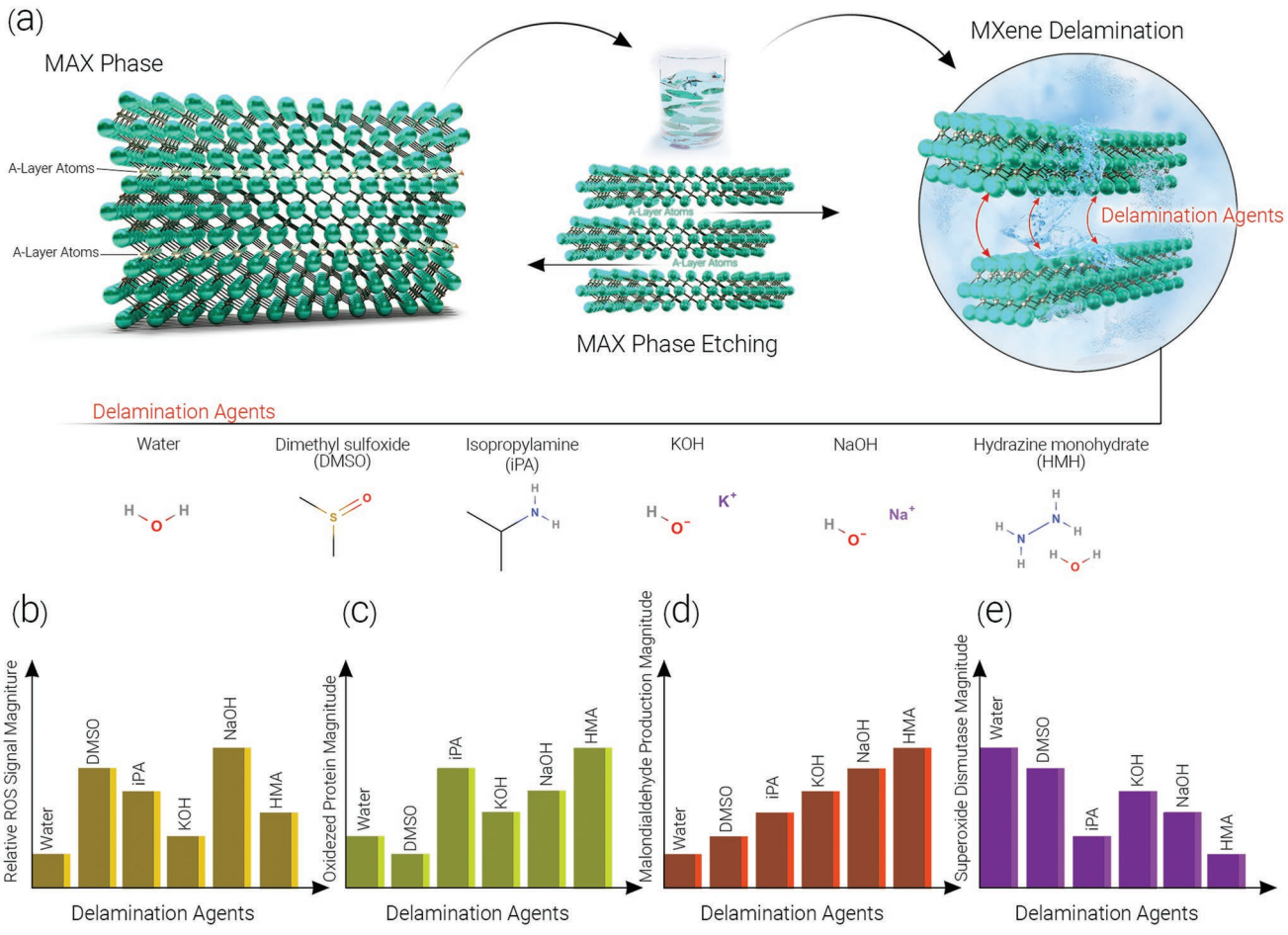

Figure 9. Schematic illustration of MAX phase structure and delamination process toward the synthesis of MXene. The effect of various delamination agents toward the synthesis of different MXenes after 3 h incubating with *E. coli* on b) the relative intracellular ROS concentrations of bacterial cells, c) the level of oxidized protein, d) relative malondialdehyde concentrations as criteria of membrane oxidation, and e) the intracellular superoxide dismutase content.[82]

for the biocidal activity of MXenes.[102,103] There is a wide range of thermal resistance among bacteria, even among those belonging to the same species.[162] There is no clear understanding of why bacteria behave in this way, and the final events leading to heat-induced bacteria inactivation are still unclear. Upon exposure to light, MXenes with high photothermal efficiency heat up,[163] leading to serious damage to nearby pathogens. In fact, the generated heat can severely affect the bacteria membrane which mainly is composed of lipids, proteins, and polysaccharides. Damaged membranes change the membrane permeability as well as intracellular homeostasis.[164,165] DNA denaturation and protein denaturation[166] are other direct effects of heat that can result in bacteria inactivation. Several studies have used the "*nanothermal blade*" expression to show the dual effect of MXenes in killing bacteria by both sharp edges and heat production.[103] Practically, hyperthermia facilitates the rupturing of the bacterial membrane by the sharp edges of MXenes. The mechanism of deactivating bacteria by the nanothermal blade MXenes was further evaluated by MD simulation.[167] It was found that penetration of the hydrophilic $Ti_3C_2T_x$ into the hydrophobic lipid membrane of bacteria is not a spontaneous process. The required energy barrier for this process depends on the direction and dihedral angles (Φ) of penetration. As shown in **Figure 10**, penetration through the corner sites and by higher dihedral angles requires less energy which is attributed to the reduction of the cell membrane tension energy and splay energy upon increasing the Φ[168] and the smaller contact area during insertion.[169]

Interestingly, the barrier force for cell membrane penetration for other nanomaterials such as gold nanoparticles (AuNPs, 250 pN),[170] CNT (0.6 nN),[171] graphene (2.2 nN)[172] are much smaller than the value required for $Ti_3C_2T_x$ (≈10 nN). This can be related to higher hydrophilicity of MXenes and less contact area between cell membranes with CNT or AuNPs compared to $Ti_3C_2T_x$. In addition, the initial calculated velocity for penetration of MXenes is much higher than that of other nanomaterials. Accordingly, the cell penetration of MXenes must happen under extreme conditions. Strong van der Waals and H-bonding interactions stick the $Ti_3C_2T_x$ nanosheets to the cell lipid membrane. Then, significant heat transfer between the $Ti_3C_2T_x$-lipids polar head interfaces upon light irradiation increases the plasma membrane temperature up to 61 °C. This high temperature prominently disturbs the plasma membrane and destabilizes it, inducing cell death.

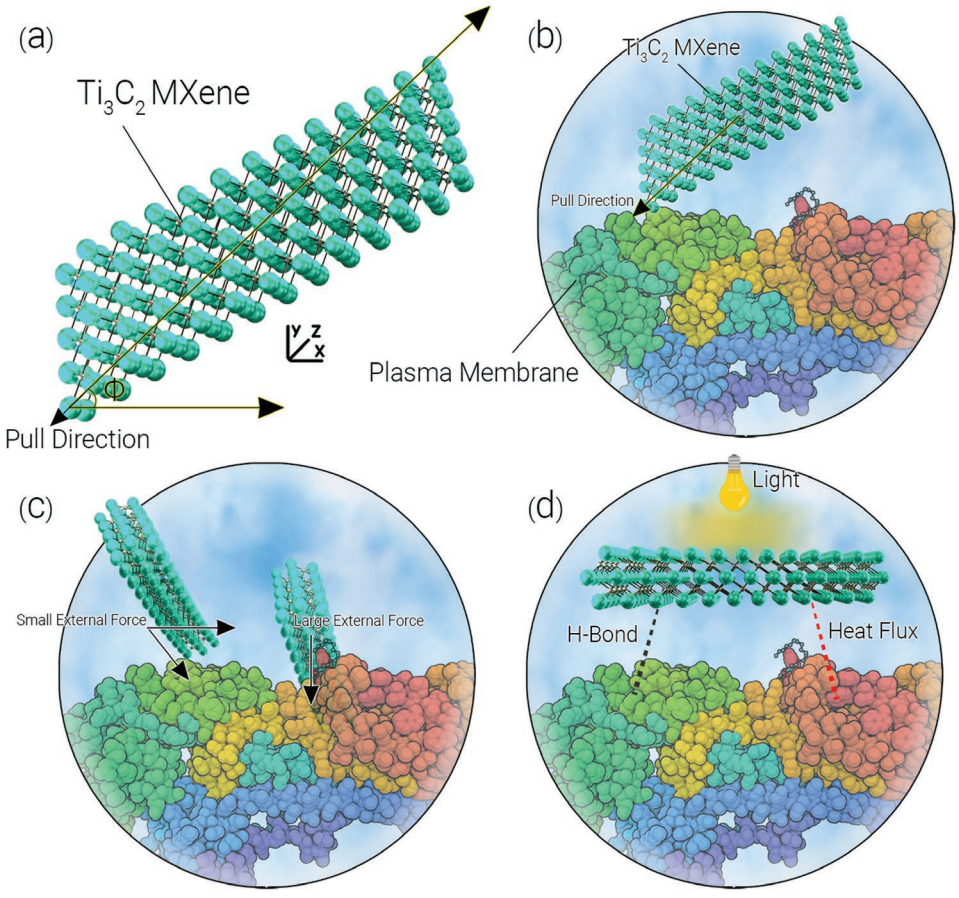

Figure 10. The critical force required for the insertion of the $Ti_3C_2T_x$ nanosheet. a) Pull force is applied to the barycenter of a single layer $Ti_3C_2T_x$ with a corner site and a smooth site toward the membrane. b) Pull direction toward the cell membrane. c) $Ti_3C_2T_x$ nanoflakes are inclined to penetrate the plasma membrane with sharp corner sites vertically with the help of an external force. d) $Ti_3C_2T_x$ nanoflake clinging to the plasma membrane with the photothermal effect.

Table 3. The schematic illustration of MXene structures that have been used as an antibacterial agent against different types of bacteria and the susceptibility method used for the evaluation. The complete details for each MXene and related studies are available in Table S1 in the Supporting Information.

Type of MXene	Type of Bacteria	Susceptibility Method
$Ti_3C_2T_X$ 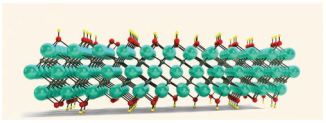	*Escherichia coli* *Bacillus subtilis*	Plate colony count Flow cytometry Fluorescence Imaging
Ti_2CT_X 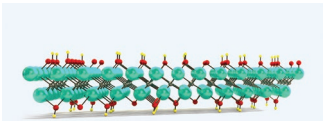	*Staphylococcus aureus* *Bacillus subtilis* *Sarcina*	Disk diffusion
V_2CT_X+NIR 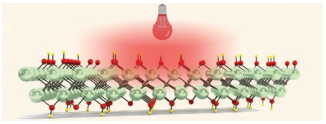	*Escherichia coli* *Staphylococcus aureus* *Bacillus subtilis* *Pseudomonas aeruginosa* *Acinetobacter baumannii* *Salmonella Typhi* *Burkholderia cepacia* *Enterobacter cloacae* *Klebsiella aerogenes* *Proteus mirabilis* *VRE* *Enterococcus faecalis* *Streptococcus agalactiae* *Klebsiella pneumoniae*	Plate colony count Disk diffusion
Nb_2CT_X+NIR 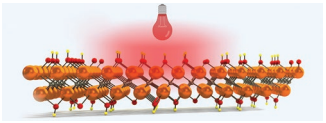		
$Ti_3C_2T_X$+NIR 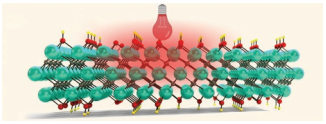		

In summary, the antimicrobial properties of MXenes include synergistic effects of both chemical and physical factors. Direct physical contact between sharp edges of nanosheets with the microbe membrane can tear up the membrane and induce the leakage of cytoplasm contents. Simultaneously, the chemical inactivation of microbes through ROS and heat generation because of light absorption by MXenes can further improve the biocidal activity of the nanosheets. Additionally, the release of low concentrations of the metal ions upon oxidation of the MXenes contributes to the deactivation of microorganisms.

4.2. The Antibacterial Properties of MXenes and MXene-based Nanocomposites

4.2.1. The Antibacterial Properties of MXenes

Among various MXenes, only Ti, Nb, and V MXenes have been studied as 2D antimicrobial nanomaterials against fungi and different types of gram (+) and gram (–) bacteria. **Table 3** and Table S1 (Supporting Information) summarize the utilized MXenes under different conditions along with the antibacterial results.

The first report on the antibacterial activity of MXenes in 2016 was related to $Ti_3C_2T_x$ against *E. coli* and *B. subtilis* using single- and few-layer $Ti_3C_2T_x$ nanosheets in colloidal solutions.[141] The results showed that delamination of the MXenes and the use of individual 2D sheets can improve antibacterial activity by increasing the surface area and sharp edges of 2D sheets. The bacterial growth inhibition for colloidal solutions of the MXene precursor (Ti_3AlC_2 MAX phase), multilayer $Ti_3C_2T_x$, and delaminated $Ti_3C_2T_x$ were <20%, ≈30%, and >97%, respectively. The antibacterial efficiency of $Ti_3C_2T_x$ was concentration-dependent (bacterial inhibition> 99% at 200 μg mL^{-1} in 4 h contact) with stronger activity against gram (+) bacteria (*B. subtilis*) than gram (–) bacteria (*E. coli*). The less effectiveness of MXene on E. coli is due to the slightly more negative surface charge of gram (–) contributing to its higher resistance to the MXene nanosheets which have negative surface charges, in agreement with the antibacterial results of other 2D nanomaterials.[173,174] Additionally, the antibacterial activity of $Ti_3C_2T_x$

was stronger than GO. However, another study indicated that delaminated $Ti_3C_2T_x$ has almost no antibacterial activity against *E. coli*,[175] which probably can be related to the difference in the morphology of the 2D sheets, sharpness of the flake edges, and their sizes. The authors did not report the lateral size of nanosheets and mentioned the need for further work to investigate the impact of flake size and the tendency of redox reactions, which can notably affect the final antibacterial properties of MXenes.

The atomic structure of MXenes can dramatically affect their biocidal activity. A thinner titanium-containing MXene, Ti_2CT_x showed no zone inhibition activity against *E. coli* whereas $Ti_3C_2T_x$ can inhibit bacterial growth. The reason was attributed to the atomic structure and stoichiometry of elements in the MXene components.[176] Similarly, Ti_2CT_x showed no biocidal activity against various gram-positive bacteria (*B. subtilis*, *S. aureus*, and *Sarcin*), indicating the important role of atomic structure and stoichiometry of the MXenes (Ti_2CT_x versus $Ti_3C_2T_x$) on their antibacterial activity.[177] In addition to antibacterial activity, it has been demonstrated that delaminated $Ti_3C_2T_x$ nanosheets have an antifungal activity to significantly inhibit the growth of Trichoderma reesei fungus.

A combination of several properties such as a 2D layered structure, excellent NIR absorption, and competent photothermal conversion properties can make the monolayer $TiVCT_x$ a robust candidate material for sterilization.[178] Nanoblades $TiVCT_x$ were synthesized by etching TiVAlC MAX using an HCl/LiF solution. The photothermal property of monolayer $TiVCT_x$ MXene was verified as the temperature of a $TiVCT_x$ solution (40 μg mL^{-1}) increased from 27 °C to ≈31 °C during 5 min under NIR laser (808 nm, 0.1 W cm^{-2}). The bacteria deactivation rate of $TiVCT_x$ against *E. coli* and *B. subtilis* [(40 μg mL^{-1}), NIR irradiation (808 nm), 30 min] was 100% and 99.8%, respectively, indicating no more negligible sterilization effect of $TiVCT_x$ compared to that of $Ti_3C_2T_x$.

4.2.2. MXene Hybrids and Composites for Improving Antimicrobial Activity

MXene active surfaces have been used for attaching different structures to further tune their antimicrobial properties. Metal and metal oxide nanoparticles, other 2D materials, and polymers have been used for endowing new properties or improving the antibacterial properties of MXenes. Hybridization of MXenes with other materials can provide synergistic effects, leading to enhanced antibacterial properties.

Hybrids with Metal and Metal Oxide Nanoparticles: Various types of nanoparticles such as SnO_2,[179] TiO_2,[180,181] Cu_2O,[182] Mn_3O_4,[183] MnO_2,[184] and Sb_2O_3[185] have been applied for modifications of MXenes. The antibacterial properties of MXenes through physically damaging bacterial membrane structure and chemically induced oxidative stress can be further promoted by combination with other antibacterial nanomaterials. A potential solution to fight against antibiotic-resistant bacteria is to develop multi-mechanism antibacterial materials with synergistic effects.[34] Table S2 (Supporting Information) provides a summary of different composites containing MXenes along with their antibacterial applications.

The simplest chemical modification of $Ti_3C_2T_x$ without applying an external modifier agent for improving the biocidal activity is the controlled oxidation of MXenes to form TiO_2 nanocrystals in the MXenes structure.[186–188] The carbon atoms in $Ti_3C_2T_x$ are converted to CO_2 and removed from the nanosheet structures in the oxidation process. It is possible to prevent the loss of carbon atoms by controlling the oxidation process so that graphitic and amorphous carbon-supported TiO_2 hybrid nanostructures with high photocatalytic activity can be obtained. Antibacterial activity against *E. coli* under light exposure for non-oxidized MXene was only around 52% which increased to 97% for graphitic carbon-supported TiO_2 hybrid nanostructures.[188] The antibacterial activities under dark conditions for non-oxidized MXene and graphitic carbon-supported TiO_2 hybrid nanostructures were around 43% and 62%, indicating the critical role of light in generating ROS for deactivating bacteria. Additionally, the killing efficiencies for pure TiO_2 against *E. coli* in dark conditions or under light exposure were around 55% and 71%, indicating the weaker photo-activity of pure TiO_2 than TiO_2-$Ti_3C_2T_x$ and MXene-based TiO_2-carbon hybrid structures due to the generation of less ROS by pure TiO_2. The enhanced photocatalytic activity was attributed to the synergetic effect between graphitic carbon and the vacancy defects in the TiO_2 nanoparticles on the MXenes nanosheets. Graphitic carbon in TiO_2 enhances carrier transfer pathways, which can facilitate charge transport.

Silver, one of the most well-known antibacterial metals,[37] has been used by several research groups to improve the biocidal activity of MXene nanosheets. Combining $Ti_3C_2T_x$ nanosheets with Ag nanoparticles provides antiseptics with excellent performances and long-term antibacterial activity.[189] In addition to acting as nanoknives, $Ti_3C_2T_x$ nanosheets provide the PTT antibacterial mode. Comparative photothermal properties showed that in response to 5 min NIR irradiation at 808 nm, the temperature of a 200 μg mL^{-1} $Ti_3C_2T_x$ suspension increased to 60 °C. In contrast, under the same condition, the Ag/$Ti_3C_2T_x$ solution temperature increased only to 50 °C. For in vivo and wound healing applications, hyperthermia can be harmful, and therefore the photothermal property of Ag/$Ti_3C_2T_x$ is enough to guarantee the fabrication of proper materials for wound healing. Interestingly, in the absence of NIR and for concentrations up to 200 μg mL^{-1}, neither Ag nor $Ti_3C_2T_x$ showed any antibacterial activity against *E. coli*, but Ag/$Ti_3C_2T_x$ showed evident bactericidal activity. On the contrary, NIR irradiation enhanced the antibacterial activity of Ag, $Ti_3C_2T_x$, and Ag/$Ti_3C_2T_x$. The effect for Ag/$Ti_3C_2T_x$ was significant at concentrations above 100 μg mL^{-1}, complete inhibition of bacterial growth was achieved. Composite Ag/$Ti_3C_2T_x$ showed a synergistic antibacterial mode of action combining PTT of MXenes with Ag^+ release. Practically, the photothermal activity of MXenes reduces the effective required dose of Ag ions and improves the biocidal efficacy.

Covering the surface of $Ti_3C_2T_x$ with Al_2O_3/Ag, SiO_2/Ag, and SiO_2/Pd through the sol-gel method increased the antibacterial

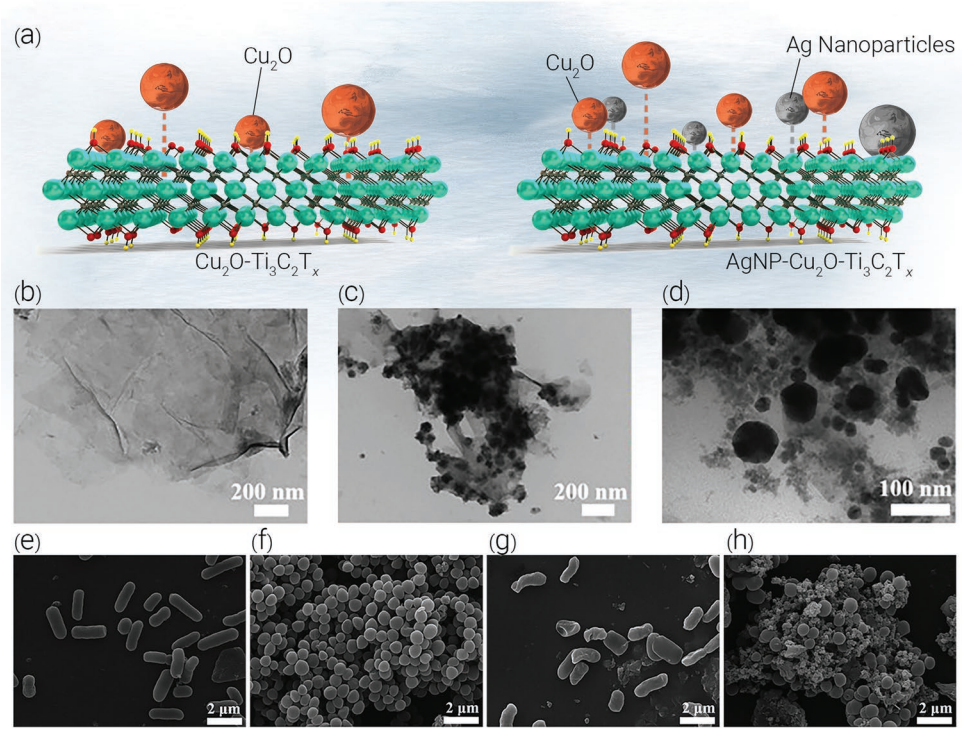

Figure 11. a) Schematic structure of Ag-$Ti_3C_2T_x$-Cu_2O nanocomposites. TEM images of b) $Ti_3C_2T_x$ nanosheets, c) $Ti_3C_2T_x$-Cu_2O nanocomposites, d) Ag-$Ti_3C_2T_x$-Cu_2O nanocomposites. SEM images of e) control *P. aeruginosa*, f) control *S. aureus*, g) Ag-$Ti_3C_2T_x$-Cu_2O treated *P. aeruginosa*, and h) Ag-$Ti_3C_2T_x$-Cu_2O treated *S. aureus P.* Adapted with permission.[191] Copyright 2020, Elsevier.

properties of MXene against both gram-positive and gram-negative bacteria.[190] The reason was attributed to the synergistic effect through possible release of Ag^+ or Pd^+ along with the PTT effect of MXenes nanosheets. MXene-based nanocomposites (Ag-$Ti_3C_2T_x$-Cu_2O) with vigorous photocatalytic bacteriostatic activity were developed through a wet chemical method (**Figure 11**a).[191] Electrostatically self-assembly between positively charged Cu (II) and Ag(I) with negatively-charged $Ti_3C_2T_x$ nanosheets leads to the complete wrapping of the nanosheets onto the nanoparticles. The generation of double charge transfer channels by the ternary nanocomposites increased the photocatalytic performance of the nanocomposite, resulting in higher ROS content. While Cu_2O nanoparticles bacteriostatic efficiencies were around 76 and 74% respectively, against *P. aeruginosa* and *S. aureus*, these efficiencies were increased to 86% against both bacteria for $Ti_3C_2T_x$@Cu_2O and to over 99% for Ag-$Ti_3C_2T_x$-Cu_2O. SEM images (Figure 11e-h) showed damage to the morphology of the bacteria upon contact with Ag-$Ti_3C_2T_x$-Cu_2O. The improved antibacterial activity originated from the synergistic effects of three factors including released Cu and Ag ions, generated ROS, and the sharp edges of $Ti_3C_2T_x$ nanosheets.

Surface modification of the $Ti_3C_2T_x$ by Cu_2O (**Figure 12**a) and their atomic interactions provided synergistic effects for antibacterial properties.[192] Zeta potentials of $Ti_3C_2T_x$ nanosheets, Cu_2O nanoparticles, and Cu_2O-$Ti_3C_2T_x$ nanosheets were around -43, +15, and -4 mV, respectively. Indeed, highly negatively charged MXene nanosheets could strongly adsorb the positive Cu_2O through tight electrostatic interactions. Comparing the biocidal activity of Cu_2O, MXenes, their physical mixture, and Cu_2O-$Ti_3C_2T_x$ (Figure 12b) demonstrates the stronger biocidal activity Cu_2O-$Ti_3C_2T_x$. The antibacterial activity of the neat MXene and Cu_2O were around 42 and 84% against *P. aeruginosa* and 56 and 85% against *S. aureus*, respectively, while the antibacterial activity of the mixture and Cu_2O-$Ti_3C_2T_x$ were around 83 and 97% against *P. aeruginosa* and 82 and 96% against *S. aureus*, respectively. The primary biocidal mechanism for Cu_2O is ROS generation. However, it is highly demolished by severe photo corrosion due to the accumulation of photo-generated electrons and holes inside the Cu_2O crystal.[193] The mechanism for synergistic antibacterial ability of Cu_2O-$Ti_3C_2T_x$ is depicted in Figure 12c. MXene can improve the separation efficiency of electron-hole pairs in Cu_2O leading to generation of more ROS for bacterial deactivation. Additionally, the surface plasmon resonance (SPR) in the local area on Cu_2O-$Ti_3C_2T_x$ surface further increases the ROS generation by enhancing the electric field. The third synergistic factor is the release of Cu (II) ions which can destroy the cell wall of bacteria. Finally, the sharp edges of MXenes can rupture the cell membrane and facilitate the diffusion of Cu(II) into the cell structure which ultimate effect is the bacteria-killing.

Gold nanoparticles could improve the antimicrobial properties of MXenes by enhancing ROS generation. For fabrication of the hybrid gold nanocomposite (AuNC)-$Ti_3C_2T_x$ structure, first, the modified $Ti_3C_2T_x$-NH_2 was prepared by functionalization of the surface of $Ti_3C_2T_x$ nanosheets (0.9 µm) with 3-aminopropyl triethoxysilane (APTES) and then gold nanoclusters (AuNCs, size < 2 nm) with -COOH groups on the surface were covalently coupled to the $Ti_3C_2T_x$-NH_2 through amide formation.[194] Comparative evaluation of the antibacterial

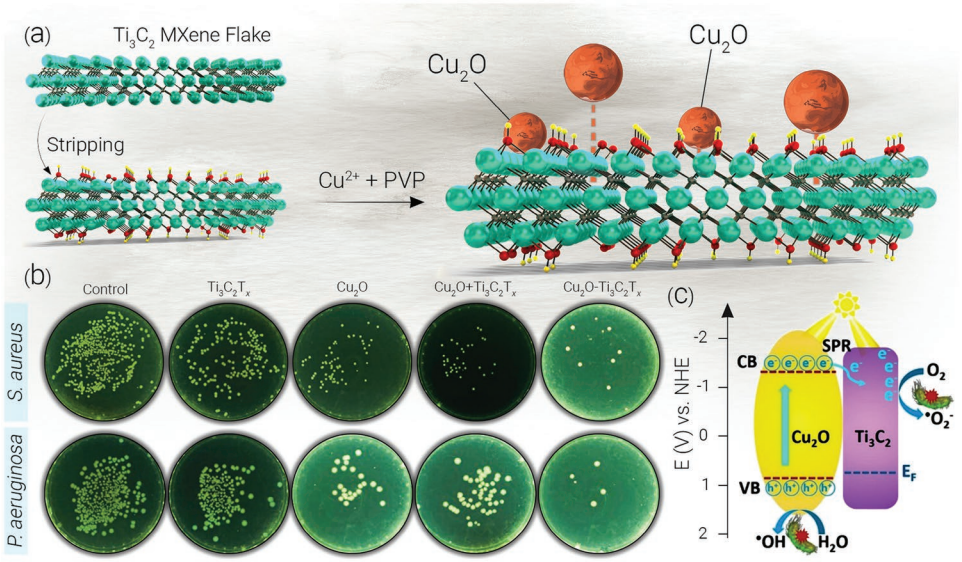

Figure 12. a) Process for fabrication of Cu_2O-$Ti_3C_2T_x$ hybrid structure. b) Antibacterial evaluation against *S. aureus* and *P. aeruginosa* after 3 days of contact for control, $Ti_3C_2T_X$, Cu_2O, the mixture of Cu_2O with $Ti_3C_2T_x$, and Cu_2O-$Ti_3C_2T_x$. c) Illustration of the charge separation process in Cu_2O-$Ti_3C_2T_X$ and its antibacterial mechanism through ROS generation. Adapted with permission.[192] Copyright 2020, Elsevier.

properties of $Ti_3C_2T_x$, $Ti_3C_2T_x$-NH_2 with AuNCs@$Ti_3C_2T_x$ (at concentration 25 μg mol^{-1}, equal to 0.085 μM AuNCs) against *S. aureus* showed the killing percentage of 40%, 44%, and >98%, respectively. The killing efficacy values against *E. coli* were around 36% and 96%, respectively, for $Ti_3C_2T_x$ and AuNCs@$Ti_3C_2T_x$. Notably, the killing efficiency of neat AuCNs for both bacteria at such a low concentration was <5% indicating the importance of the synergistic effects in the structure of AuNCs@$Ti_3C_2T_x$. The IC_{50} for neat $Ti_3C_2T_x$ and AuCNs for *S. aureus* were around 32.2 μg mL^{-1} and 2.4 μM, which, respectively, reduced to 11.7 μg mL^{-1} and 0.04 μM for AuNCs@$Ti_3C_2T_x$. Despite the very low content of gold, the ROS generation by AuNCs@$Ti_3C_2T_x$ was more than two times higher than that for $Ti_3C_2T_x$. In this low concentration, neat AuNCs generate a meager amount of ROS, which cannot be the origin of antibacterial activity. Furthermore, the crumpled AuNCs@$Ti_3C_2T_x$ could prevent biofilm formation. A combination of physical (by MXenes) and chemical (by MXenes and AuNCs) antibacterial mechanisms was responsible for the ultimate antibacterial activity of this composite. The sharp edges of MXenes can physically rupture the cell membrane and facilitate the internalization of AuNCs into the bacteria cell to produce localized ROS, which can result in lipid membrane and DNA oxidation and finally bacterial death. A NIR-activated heterostructure catalyst composed of 2D $Ti_3C_2T_x$ and 1D cobalt nanowires (CoNWs) with improved antibacterial activity was developed by Liu et al.[195] The NIR absorption capability at 808 nm for $Ti_3C_2T_x$/CoNWs was a little stronger than that of the neat $Ti_3C_2T_x$, which was attributed to the d-d transition of Co that improves the light absorbance. Additionally, the photoluminescence (PL) intensity of $Ti_3C_2T_x$/CoNWs was weaker than that of the pristine $Ti_3C_2T_x$ indicating inhibition of the electron-hole recombination in $Ti_3C_2T_x$/CoNWs. These results lead to the higher ROS generation by $Ti_3C_2T_x$/CoNWs compared to $Ti_3C_2T_x$, which implied the more robust photocatalytic activity of MXenes after modification by CoNWs. Furthermore, the photothermal property of the $Ti_3C_2T_x$/CoNWs was higher than that of pristine $Ti_3C_2T_x$. As a result, the temperature of $Ti_3C_2T_x$/CoNWs coated on the surface of sulfonated polyether ether ketone (PEEK) increased by 7 °C than $Ti_3C_2T_x$ upon 808 nm NIR irradiation for 20 min. In the dark condition, both $Ti_3C_2T_x$/CoNWs and $Ti_3C_2T_x$ showed almost no antibacterial activity. In contrast, upon NIR laser (808 nm, 1.5 W cm^{-2}) irradiation for 20 min, $Ti_3C_2T_x$ showed 40% and 25% antibacterial activity against *S. aureus* and *E. coli*, respectively. Respectively, the killing efficiencies increased to 92% and 80% for $Ti_3C_2T_x$/CoNWs. A synergetic NIR-induced PTT/photodynamic therapy (PDT) was mentioned for the antibacterial mechanism of $Ti_3C_2T_x$/CoNWs. The NIR irradiation increased the bacterial membrane permeation by photothermal-induced hyperthermia and then generated ROS by NIR passed through the bacterial membrane easily which results in oxidative stress and leakage of the bacterial protein.

MXene/other 2D Composites: 2D MoS_2 nanomaterials vertically aligned on $Ti_3C_2T_x$ MXene were used as antibacterial material against gram(+) and gram(-) bacteria.[196] MoS_2 has demonstrated robust antibacterial activity.[197,198] MXene nanosheets with a thickness of ~ 1 nm (monolayer) to 350 nm (multilayer) were used for vertically tethering 100 nm flower-shape MoS_2 through the thermal treatment of $(NH_4)_2MoS_4$. The immobilized MoS_2 nanosheets act as nanoknives to tear down the bacteria membrane, which leads to the release of cytoplasmic materials and bacteria death (**Figure 13**). However, the thicker PM (peptidoglycan mesh) layer in gram (+) bacteria increased its resistance against MoS_2/ $Ti_3C_2T_x$ nanocomposite.

MXene with GO sheets have also been studied for antibacterial applications. To enhance 3-hydroxybutyrate-co-hydroxyvalerate (PHBV) use in biological applications, it is important to make it hydrophilic and antibacterial. To achieve these, MXene/GO composites were grafted on PHBV.[199] Excellent hydrophilicity and 2D structure with very thin thickness

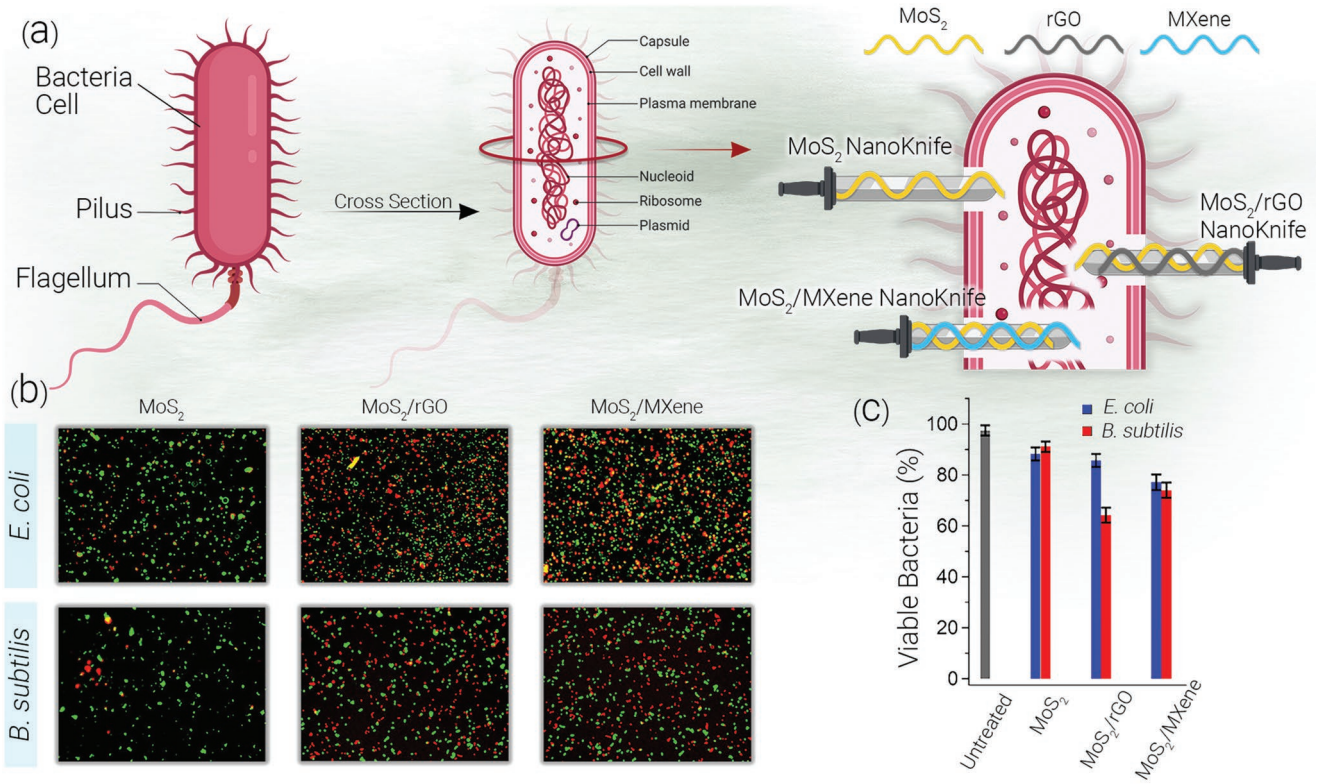

Figure 13. a) The schematic illustration of bacteria cell and nanoknife mechanism. b) Fluorescence imaging, and c) flow cytometry results of the antibacterial activity of MoS_2, MoS_2/rGO, and MoS_2/MXene nanomaterials against *E. coli* and *B. subtilis* bacteria (conditions: 100 μg mL^{-1} of the nanomaterials for 3 h contact time under dark condition). Adapted with permission.[196] Copyright 2018, American Chemical Society.

and ROS generation provided by GO and MXene result in high hydrophilicity of the nanocomposites (PHBV/MXene/GO) with robust microbial activity (97%). As expected, increasing the content of GO/MXene to 1.0 wt.% enhances the inhibition effect significantly.

The Antibacterial Properties of Organic-Coated MXenes: Like other nanomaterials, coating the surface of MXenes nanosheets with polymers is another strategy for providing materials with more robust biocidal activities. However, this modification of MXenes to improve biocidal activity has not developed extensively.

Coating poly(L-lysine) (PLL) on MXenes can reverse the charge of the nanosheets, which results in a direct effect on the biocidal activity of MXenes. Functionalization of the negatively-charged surface of 2D $Ti_3C_2T_x$ flakes by the cationic PLL through electrostatic adsorption reverses the charge of the flakes to become positive up to + 40 mV at a $Ti_3C_2T_x$:PLL weight ratio of 1:4.[138] Additionally, this simple modification could reduce the size of the MXene flakes from 800 nm to around 300 and 100 nm using MXene: PLL weight ratio 1:1 and 1:4, respectively. Unlike other studies, the authors observed no antibacterial activity against *E. coli* for the unmodified $Ti_3C_2T_x$, which was attributed to the negative charge of the MXene and its aggregation in aqueous solutions, as in this study the authors made a $Ti_3C_2T_x$ with relatively close to zero zeta potential, unlike the typical $Ti_3C_2T_x$ MXenes. Their 2D $Ti_3C_2T_x$/PLL with a positive charge and less aggregation at 200 μg mL^{-1} concentration could significantly retard the *E. coli* growth.

5. Applications of MXene as an Antibacterial Agent

Dealing with antibacterial infections is essential in many areas. MXene-based antibacterial materials have been explored mainly in wound dressing, water purification membranes, and solar-driven water purification systems.

5.1. Fabrication of Wound Dressings

Hydrogels and electrospun fibers are proper candidates for wound dressing applications, and therefore, various types of antibacterial hydrogels[200–204] and electrospun fibers[205] have been developed for treating wound infections. MXenes as biocompatible materials have been applied to endow antibacterial properties to these types of wound dressings.[206]

Electrospun chitosan (CS)-bandages incorporated by MXenes were applied as antibacterial wound dressing membranes.[131] The MXenes could uniformly disperse on the nanofiber surface. The glutaraldehyde-crosslinked MXene/CS nanofiber mates showed a bacterial reduction of around 95 and 62% against *E. coli* and *S. aureus* compared to the control CS fibers. The thicker peptidoglycan cell wall of gram(+) *S. aureus* was the main reason for its stronger resistance against antibacterial sharp edge agents.[207] In addition to antibacterial activity, these mats showed appropriate biocompatibility with cell viability of over 85% against HeLa cells after 72 h exposure. The

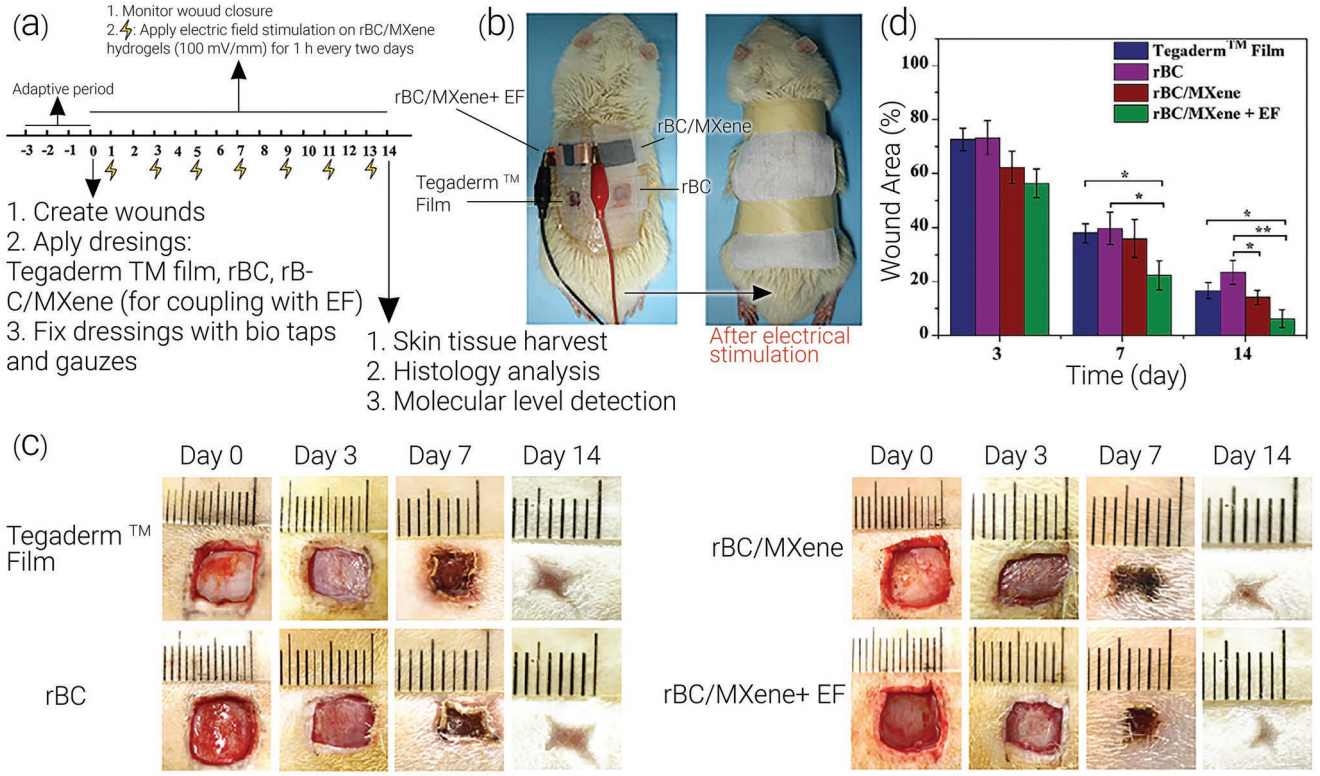

Figure 14. a) Illustration of in vivo wound healing process. b) Photographs for the wounds in Sprague-Dawley (SD) rats treated with different dressings. c) Images of wounds on different days after treatment with commercial Tegaderm wound film, rBC, and rBC/MXene nanocomposite in the presence/absence of an external electric field (EF). d) Wound area after different times treated by various dressings. Reproduced with permission.[206] Copyright 2020, Wiley-VCH.

porous nanocomposite hydrogels of $Ti_3C_2T_x$/chitosan/hyaluronate containing 5 wt.% MXene could deactivate >99% of *E. coil* and *S. aureus*.[208] Addition of multilayer $Ti_3C_2T_x$ MXene to a solution of regenerated bacterial cellulose (*r*BC) in the NaOH/urea/water system and then crosslinking with epichlorohydrin leads to $Ti_3C_2T_x$/*r*BC nanocomposite hydrogel.[206] The growth of NIH3T3 cells on these nanocomposite hydrogels was even better than neat *r*BC, indicating no cytotoxicity and excellent biocompatibility. Furthermore, the wound closure by a $Ti_3C_2T_x$/rBC composite hydrogel dressing was faster than the neat *r*BC (**Figure 14**). Additionally, by exposing an external electrical stimulation, the proliferation activity of cells improved and faster wound closing was obtained.

A self-healing, electrical conductive, and tissue-adhesive MXene-based hydrogel with strong antibacterial and hemostatic properties and good biocompatibility was developed to treat methicillin-resistant *S. aureus* (MRSA)-infected wounds.[209] This multifunctional scaffold was prepared by the Schiff-base crosslinking reaction of a mixture of branched poly(glycerol-ethylenimine) (PEIG), polydopamine-modified MXene nanosheets (PDA/MXene), and oxidized hyaluronic acid. This hybrid hydrogel with 0.53w% $Ti_3C_2T_x$ MXene showed effective antibacterial activity against *E. coli*, *S. aureus*, and MRSA with growth inhibitions of around 98.6, 99.9, and 99.0%, respectively, indicating more potent biocidal properties than well-known antibiotics such as ampicillin (**Figure 15**a). Furthermore, a cytotoxicity test against L929 cells at the concentrations of 5–25 µg mL^{-1} showed excellent biocompatibility of this hydrogel with cell viability of over 99% (Figure 15b) which makes it a proper material for biomedical applications. Comparison of the closure of MRSA-infected wounds in mice after dressing with blank, commercial 3M hydrogels, PEIG/oxidized hyaluronic acid hydrogel, and hybrid hydrogel (Figure 15c), respectively, revealed a reduction of around 37, 12, 34, and > 75% of the wound size after 7 days indicating the excellent anti-infection wound healing performance of the hybrid hydrogel.

A multifunctional MXene-containing implant hydrogel was developed by Yin et al. to treat osteosarcoma and bacterial infection.[210] In the first step, the MXene nanosheets were functionalized with tobramycin (TOB), an antibacterial drug with positive charges, through electrostatic interactions. Finally, a mixture of TOB@MXene was coated on the surface of the sulfonated PEEK in the presence of dopamine and then soaked in an aqueous solution of gelatin methacrylate (GelMA) in the presence of a photoinitiator and exposed to UV irradiation for the formation of a crosslinked hydrogel. This hybrid structure showed intense antibacterial activity against *E. coli* and *S. aureus* (**Figure 16**a) due to a combination of cell wall damage by the sharp MXene nanosheets and damage to the mRNA of bacteria by tobramycin (TOB). Furthermore, the presence of the MXene adds photothermal property of the hydrogel so that temperature could increase >60 °C by 10 min irradiation at 808 nm (Figure 16b), killing cancer cells (Figure 16c).

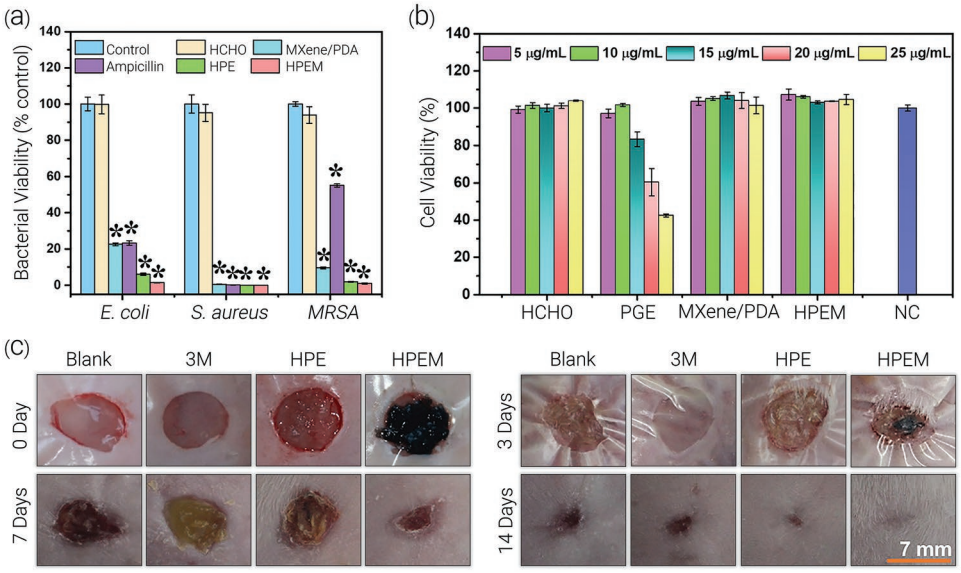

Figure 15. a) Antibacterial activity of different samples against *E. coli*, *S. aureus*, and *MRSA*. (HCHO = oxidized hyaluronic acid; HPE = poly(glycerol-ethylenimine)/oxidized hyaluronic acid hydrogel; PDA = polydopamine). b) Cytotoxicity of HPEM scaffolds against L929 cells at different concentrations for 24 h (NC = control). c) Photographs of MRSA-infected wounds in mice after different days treating with commercial 3 M, HPE, and HPEM dressings. Reproduced with permission.[209] Copyright 2021, American Chemical Society.

Chen et. al developed an injectable thermosensitive niobium carbide (Nb_2CT_x)-based hydrogel (Nb_2C@Gel) with antioxidative and antibacterial properties for diabetic wound healing.[211] The hydrogel was prepared by mixing a cold aqueous solution of poly(lactic acid-co-glycolic acid)-b-poly(ethylene glycol)-b-poly(lactic acid-co-glycolic acid) (PLGA-PEG-PLGA) triblock copolymer with a cold aqueous dispersion of Nb_2CT_x nanosheets (an average size of 153 nm, a zeta potential of –47 mV) followed by increasing the mixture temperature to 37 °C. The hydrogel exhibited good biocompatibility with keratinocytes, fibroblasts, and endothelial cells, three main cells in wound healing. The Nb_2CT_x nanosheets at a concentration of 40 μg mL^{-1} showed poor antibacterial activity in the absence of light, but upon NIR laser (808 nm) irradiation for 5 min temperature could increase to 48 °C leading to death of 90% for *S. aureus* and 81% for *E. coli*. The diabetic wound in mice treated by Nb_2C@Gel showed complete closure in 17 days whereas the ones treated by control or hydrogel (without Nb_2CT_x) remained exposed after 17 days.

In situ growth of zeolite imidazole framework-8 (ZIF-8) on the surface of $Ti_3C_2T_x$ and subsequent electrospinning with a polylactic acid (PLA) solution leads to membranes with NIR-regulated high PTT/photodynamic therapy (PDT) properties for healing wounds infected by methicillin-resitant S. aureus (MRSA) (**Figure 17**a,b).[212] While MXene has a negative surface charge, coating by ZIF-8 reversed the charge to a positive value. NIR irradiation of ZIF-8/MXene hybrid dispersion in water (100 mg L^{-1}) could increase the temperature to 56 °C in 10 min with a photothermal convention efficiency of 80%. Hyperthermia and ROS generation under NIR irradiation lead to bactericidal rates over 99.8% for both *E. coli* and MRSA for the MXene/ZIF-8/PLA membrane. In vivo investigation of MRSA-infected skin wounds in Kunming mice revealed > 99% healing of the wound treated by NIR-irradiated ZIF-8/MXene/PLA membrane, whereas the wounds treated only by NIR or ZIF-8/MXene/PLA membrane showed < 90% healing during the same period (Figure 17b). Figure 17c summarizes the wound healing process using antibacterial aids.

Grafting Nb_2CT_x MXene on the surface of a titanium plate (TP) implant provides a hybrid Nb_2CT_x@TP implant with strong anti-infection properties.[213] Under NIR irradiation, the temperature of this material could increase to 70 °C in 2 min indicating its solid photothermal properties. The formation of bacterial biofilms from MRSA and *E. coli* on Nb_2CT_x@TP were, respectively, around 190 and 74 times lower than those of the pristine TP, indicating the intrinsic biofilm resistance of the hybrid material. However, the antibacterial performance was boosted in the presence of NIR irradiation due to the strong photothermal property of the Nb_2CT_x@TP composite. In vivo evaluation of the Nb_2CT_x@TP implant against the eradication of MRSA infection in the mouse model showed that in the presence of NIR (808 nm), this implant can effectively kill the bacteria in vivo. Furthermore, it alleviates the inflammation in the damaged tissue and, therefore, improves angiogenesis and tissue regeneration.

5.2. Fabrication of Anti-biofouling Membranes for Water Purification

Biofouling is one of the main drawbacks of water separation membranes,[214] and therefore, the development of antimicrobial membranes has been proposed to address the biofouling issue during the water treatment process.[215,216]

Incorporating MXenes in the structure of membranes can provide membranes with improved anti-biofouling performances due to the potent antimicrobial activity of MXenes nanosheets. Rasool et al. prepared antifouling MXene-based

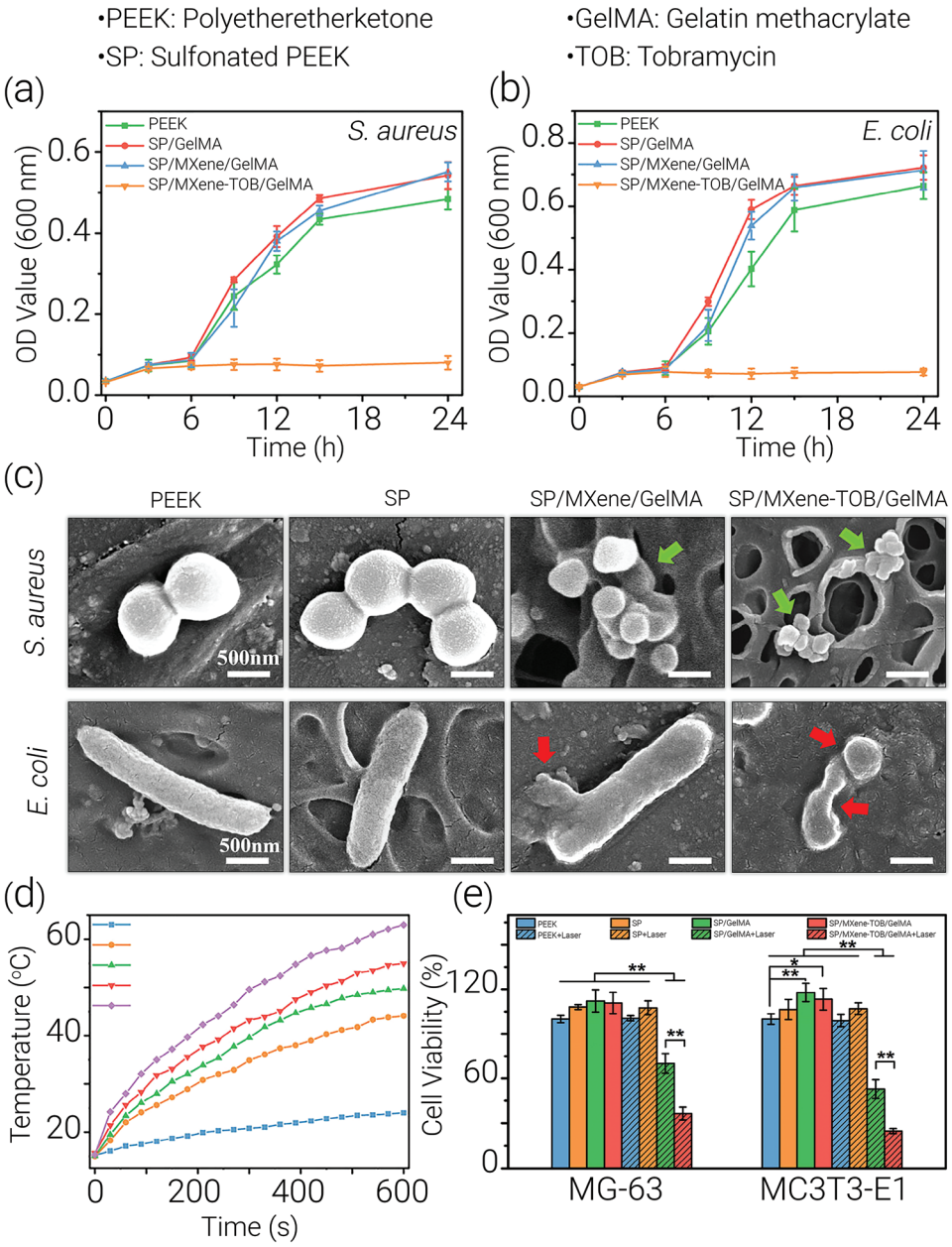

Figure 16. Bacterial growth of a) *S. aureus* and b) *E. coli* after treatment with PEEK, methacrylate SP/GelMA, SP/MXene/GelMA, and SP/MXene-TOB/GelMA. (PEEK = polyether ether ketone; SP = sulfonated PEEK; MX = MXenes; GelMA = gelatin methacrylate; MX-TOB = tobramycin-modified MXene). c) SEM images of *S. aureus* and *E. coli* after treatment with materials. d) Photothermal performance of SP/MXene-TOB/GelMA containing different concentrations of MX-TOB. e) Anti-tumor test of different scaffolds against Human osteosarcoma cancer cell line MG-63 and murine preosteoblastic cancer cell line MC3T3-E1 with and without irradiation. Reproduced with permission.[210] Copyright 2020, American Chemical Society.

membranes by filtering a dilute colloidal single-layer $Ti_3C_2T_x$ nanosheet solution on polyvinylidene fluoride (PVDF) membranes.[131] The high aspect ratio of the nanosheets guarantees the formation of uniform 2D nanochannels and reduces the formation of meso- and macro-pores across the membrane. While the neat PVDF membrane showed hydrophobicity having a water contact angle of 81°, modifying with MXene increased the hydrophilicity significantly to a contact angle of 37°. Additionally, the presence of MXene wrinkles and edges increased the roughness of the PVDF membrane. The MXene@PVDF membranes showed growth inhibition of 73% for *B. subtilis* and 67% for *E. coli* compared to the control PVDF with no activity. Increasing the thickness of the MXene layer showed no effect on the antibacterial activity indicating the surface deactivation of bacteria. As discussed before, aging of the hybrid membrane is in favor of the antibacterial activity. The density of the growing bacteria on the surface of MXene@PVDF membranes was lower than PVDF, and the bacteria were damaged

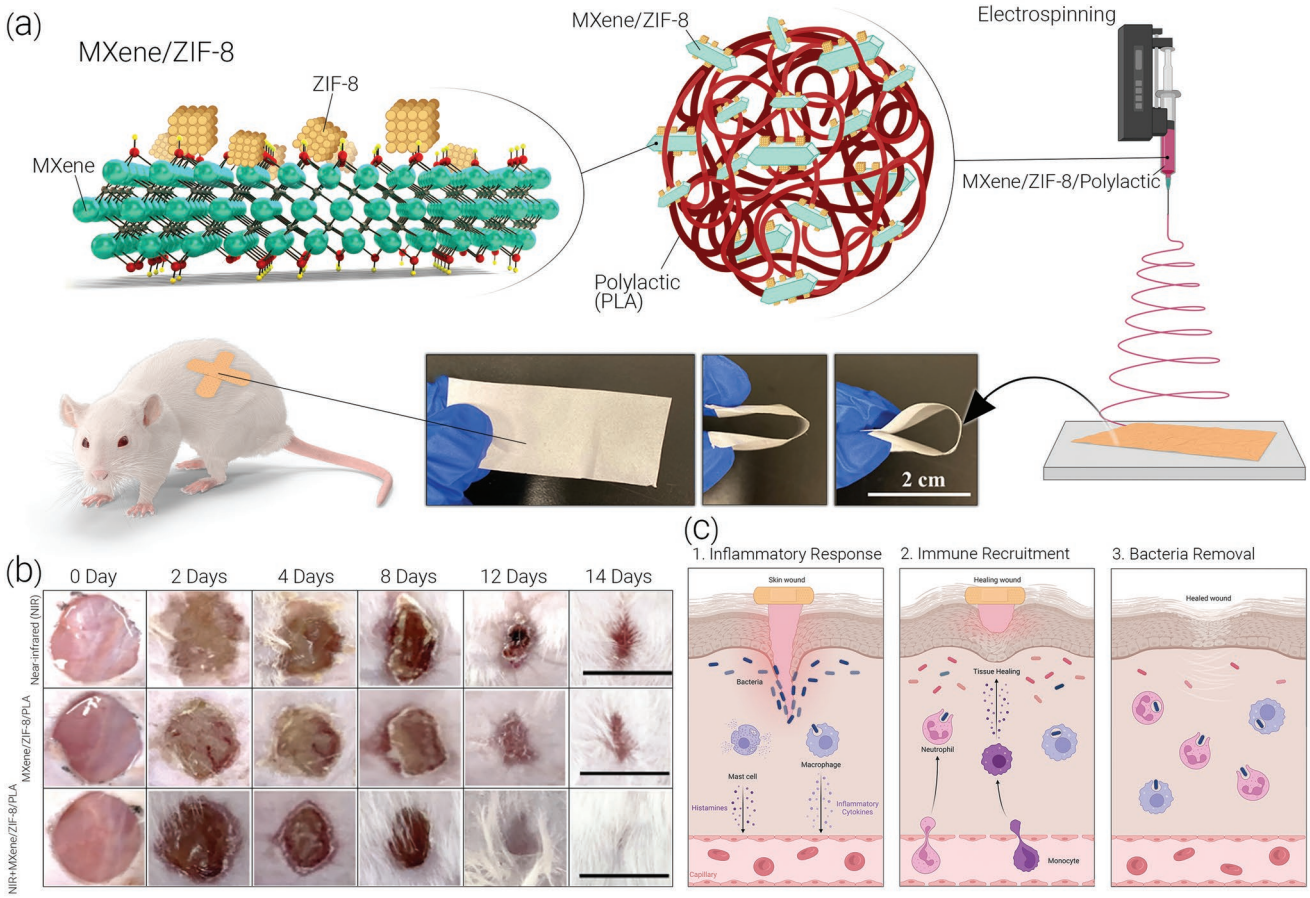

Figure 17. a) Fabrication of MXene/ZIF-8/PLA electrospun membranes for wound dressing. b) Optical photographs of wound healing process treated by (I) NIR, (II) MZ-8/PLA and (III) MZ-8/PLA + NIR with 808 nm laser treatment for 5 min (scale bar: 10 mm). c) The schematic illustration of bacteria-infected would healing process. Apated with permission.[212] Copyright 2021, Elsevier.

significantly by the MXene layer. $Ti_3C_2T_x$ nanosheets could rupture the bacterial membrane and kill the bacteria. Therefore, the MXene membrane prevents bacterial growth and biofilm formation, which is crucial in water purification membranes.

The addition of silver nanoparticles (AgNPs) to the MXene membrane was used to improve the antifouling and water flux properties.[44] The Ag@$Ti_3C_2T_x$ hybrid membrane was produced by self-reducing $AgNO_3$ into AgNPs by the $Ti_3C_2T_x$ nanosheets as a reducing agent, followed by vacuum-assisted filtration on a PVDF support. The antibacterial evaluation against *E. coli* at 35 °C for 24 h revealed the bacteria growth inhibition of around 0, 60, and > 99% for PVDF, MXene@PVDF, and Ag@MXene@PVDF, respectively. Also, AgNPs, by generating slit interspacing (1–4 nm) between the MXene nanosheets, produce nanopores in Ag@MXene@PVDF, leading to improved water flux. Effective rejecting of large molecules, including bacteria by nanopores, and excellent anti-biofouling preparties thanks to the antibacterial activity of Ag@MXene are essential factors for inhibiting the reduction of water flux of the membranes.

Coating PVDF membranes with delaminated $Ti_3C_2T_x$ through vacuum filtration improved the antibiofouling performance.[82] In that study, the effect of different exfoliation agents for $Ti_3C_2T_x$ (**Figure 18** top panel) was also considered. The water contact angle, water flux, and estimation of biofilm formation by comparing the corresponding optical densities (OD) are depicted in Figure 18. MXenes improved the hydrophilicity of the membrane significantly (Figure 18a), with the best performance for hydrazine-delaminated $Ti_3C_2T_x$ with a water contact angle of ≈40°. While coating the PVDF membrane with hydrazine-delaminated $Ti_3C_2T_x$ reduced the water flux slightly (Figure 18b), it improved the antibiofouling significantly (Figure 18c), which is a critical factor for long-term use of the membrane.

While membranes are applied for water purification through the filtration process, aerogels are another alternative for water purification through the adsorption of pollutants.[217] Aerogels composed of APTES-modified $Ti_3C_2T_x$ nanosheets, polyethyleneimine, and sodium alginate crosslinked by epichlorohydrin were applied as porous antibacterial materials for water treatment.[218] In addition to the removal of Cr (IV) and Congo Red dye as pollutant components from the aqueous medium, this aerogel showed a killing efficiency of over 99.99% against both *E. coli* and S. *aureus* after only 2 h incubation. Indeed, this multifunctional aerogel can simultaneously remove metallic and organic pollutants from the water along with sterilization of water by killing microorganisms.

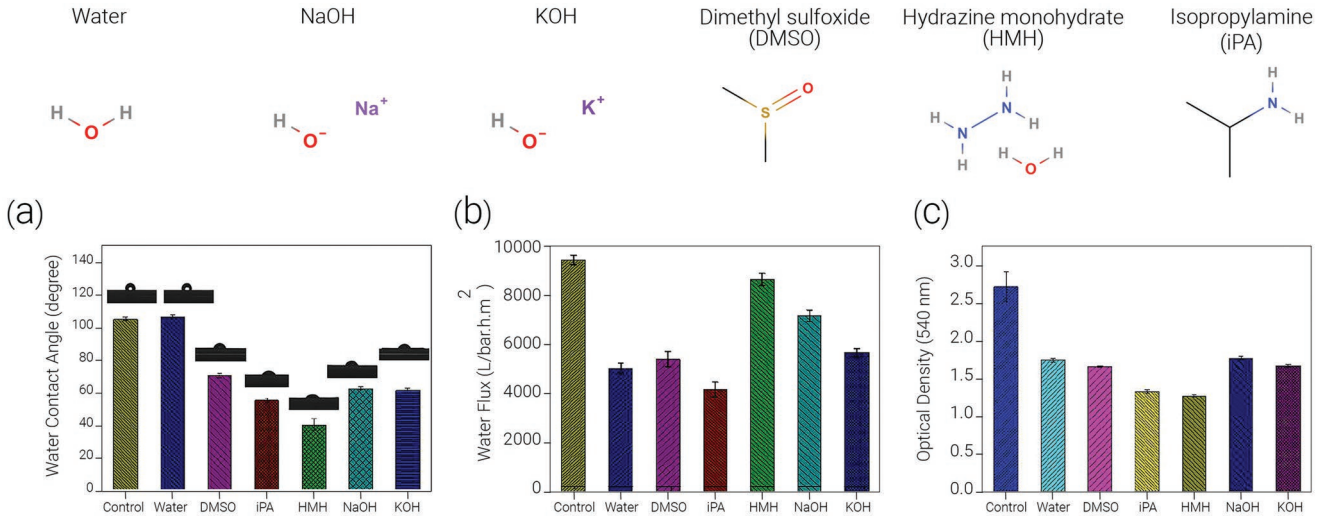

Figure 18. a) Static water contact angles, b) Water flux, and c) estimation of the biofilm formation through comparing the OD values in PVDF membranes before and after coating with differently exfoliated $Ti_3C_2T_x$.[82] (Abbreviations: DMSO = dimethyl sulfoxide, iPA = isopropylamine, HMH = hydrazine monohydrate)

5.3. Fabrication of Solar-Driven Water Purification by Antibacterial MXenes

Solar evaporation technology is a facile, green, and sustainable strategy for the production of potable water by utilizing solar energy for heating and production of vapor at temperatures lower than the boiling temperature of water.[219,220] One of the main challenges in these systems is the low photothermal conversion efficiency (30–45%) due to weak solar adsorption and significant heat losses. Different strategies such as improving light adsorption, reducing heat loss, and fabrication of more porous hydrophilic materials have been used to improve steam generation efficiency.[221] One of the most promising strategies is the development of two-layer structures in which a porous membrane with an upper photothermal surface is floating on the water.[222] Effective heat localization on the top surface of the membrane can evaporate a thin film of water with a high yield.[223,224] The photothermal property of MXenes makes them proper candidates to be applied for the fabrication of membranes for solar-driven water steam generation.[95,225,226]

Additionally, the antibacterial properties of MXenes can lead to the fabrication of sterilized purified water and prevent biofouling on the evaporator surface. A flexible MXene/cellulose photothermal membrane with excellent light adsorption and anti-biofouling properties was developed by dip-coating cellulose membrane into a $Ti_3C_2T_x$ MXene dispersion for effective solar steam generation (**Figure 19**a,b).[227] MXene nanosheets could create a smooth nanolayer on the surface of cellulose fibers. Comparative results showed that the light adsorption of MXene/cellulose membrane in the range of 300–1500 nm was 94%, whereas, for the analogous GO/cellulose membrane, it was around 87% (Figure 19c). Additionally, the surface temperature of the membrane after floating in water reached around 45 and 33 °C after 10 min solar illumination, respectively, for MXene/cellulose and GO/cellulose membranes (Figure 19d). The evaporation rate and solar steam efficiency under the solar illumination of 1 sun were around 1.44 kg m^{-2}.h and 86% for MXene/cellulose membrane. In contrast, the values were around 0.45 kg m^{-2}.h and 54% for GO/cellulose membrane (Figure 19e). Anti-biofouling results showed the production of aggregates of bacteria on the surface of neat cellulose and GO/cellulose membranes, whereas negligible bacteria were attached to the MXene/cellulose surface. The strong antibacterial properties of MXene/cellulose membrane (99.99% for *E. coli* and 99.98% for *S. aureus*) (Figure 19f–i) endow effective anti-biofouling properties in the MXene-cellulose membranes.

Ag nanoparticles modified MXene nanosheets/polyacrylonitrile (Ag@MXene/PAN) electrospun nanofiber was another solar steam generation system with excellent antibacterial properties and evaporation performance.[228] The UV–Vis-NIR light absorption efficiency for MXene/PAN and Ag@MXene/PAN nanofibers reached around 83 and 93%, respectively. Under 1 sun illumination, the surface temperature of PAN, MXene/PAN, and Ag@MXene/PAN nanofiber membranes could increase to around 36, 49, and 57 °C, respectively. In turn, the evaporation rates of 1.51 and 1.36 kg m^{-2}.h and solar vapor conversion efficiencies of 81 and 92% were reported, respectively, for MXene/PAN and Ag@MXene/PAN nanofiber membranes. Furthermore, the strong antibacterial activity of the Ag@MXene/PAN membrane (99.9% against *E. coli*) can effectively prevent biofouling formation on the surface of the membrane, reducing the efficiency of the solar evaporator system.

5.4. Miscellaneous Applications of Antibacterial MXenes

Dip coating of an aluminum sheet in a water/ethanol mixture of γ-glycidoxypropyltrimethoxysilane (γ-GPS), tetraethyl orthosilicate (TEOS), and MXenes and subsequent heating curing generated an MXene/silane film on the surface of the Al sheet with a thickness of 13 µm and excellent antibacterial

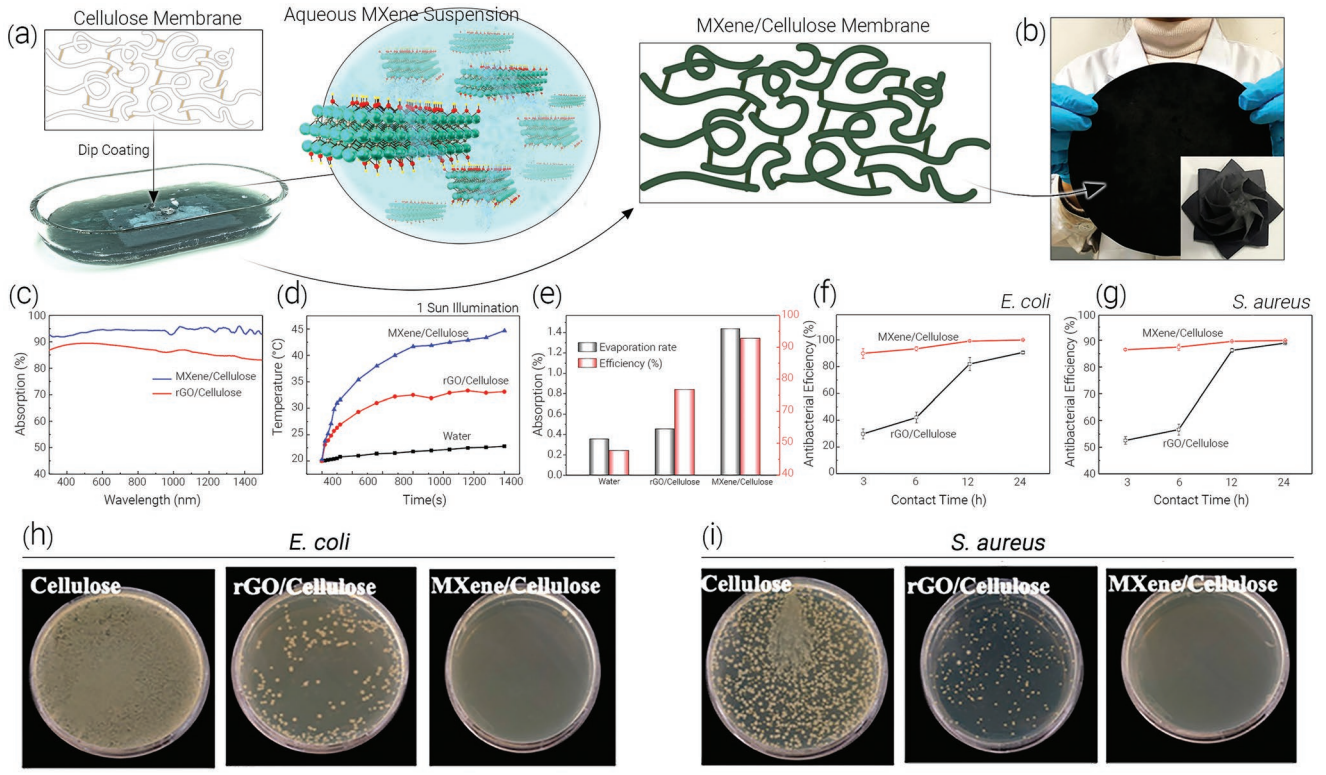

Figure 19. a) Schematic description for the fabricated anti-biofouling MXene/cellulose membrane steam generator. b) Photograph of MXene/cellulose membrane with good flexibility. c) Adsorption of light by MXene/cellulose and GO/cellulose membranes in the wet state. d) Increasing the temperature of the water, the surface of MXene/cellulose, and GO/cellulose membranes under 1 solar sun illumination at different irradiation times. e) Water evaporation rate and evaporation efficiency for water, the surface of MXene/cellulose, and GO/cellulose membranes under 1 solar sun illumination. f–i) Antibacterial efficiency of MXene/cellulose and GO/cellulose membranes against *E. coli* and *S. aureus*. Adapted with permission.[227] Copyright 2019, American Chemical Society.

and anticorrosion properties.[229] In the absence of MXenes, the generated films showed microcracks; however, by introducing MXene, these microcracks were not observed, indicating the positive effect of MXene in improving the compact structure of the coating. Since microbial corrosion from various microorganisms plays an essential role in the corrosion of metals,[230] therefore, fabrication of antimicrobial coating for metals can address this issue. While near γ-GPS/TEOS coating showed almost no antibacterial activity against *E. coli*, the hybrid coating containing MXene could almost deactivate all *E. coli*.

Coating the surface of Spandex yarn textiles with polydopamine (PDA) followed by coating with MXene/Ni^{2+} lead to conductive MPNi/Spandex coating as a wearable health monitoring dressing with antibacterial properties (**Figure 20**a).[231] This coated composite, which has a high sensitivity (5.7×10^4 gauge factor), low detection limit (0.11%), and wide sensing range (0.11 to 61.2%), can be used as strain sensors to monitor biological activities at both large and small scales. Strong photothermal properties of MXenes lead to a temperature increase of MPNi/Spandex coating to 95 °C in 10 s and 98 °C in 1 min upon NIR irradiation (808 nm, 1.25 W cm^{-2})(Figure 20b). Importantly, by tuning the intensity of the NIR irradiation, it was possible to adjust the surface temperature of MPNi/Spandex coating (Figure 20c). Additionally, this composite coating showed solid antibacterial properties (99.9% killing efficacy against *E. coli*) in the presence of NIR irradiation (Figure 20d). Synergistic effects between MXenes, PDA, and, Ni^{2+} were responsible for providing this vigorous biocidal activity, so the absence of any of these components in the coating afforded weaker biocidal activity.

6. Cytotoxicity and Environmental Impacts of MXenes

Based on the applications mentioned in the previous sections for MXenes-based antimicrobial agents, biocompatibility and having environmentally friendly characteristics are crucial for biomedical and environmental applications. MXenes wastes can be released into environments and exposed to our body through skin, respiratory and gastrointestinal systems. It is already reported that various types of other nanomaterials such as graphenes[232] and CNTs[233] can create toxicity for tissues and live organisms. Therefore, the practical applications of MXenes need to take into consideration for possible toxicities. There are several comprehensive reviews reporting the recent progress on the cytotoxicity evaluation of MXenes.[234–236] Some reports attributed the cell cytotoxicity of MXenes to the oxidative stress induced by the generated ROS. On the other hand, there are other studies reporting higher cytotoxicity of MAX phases

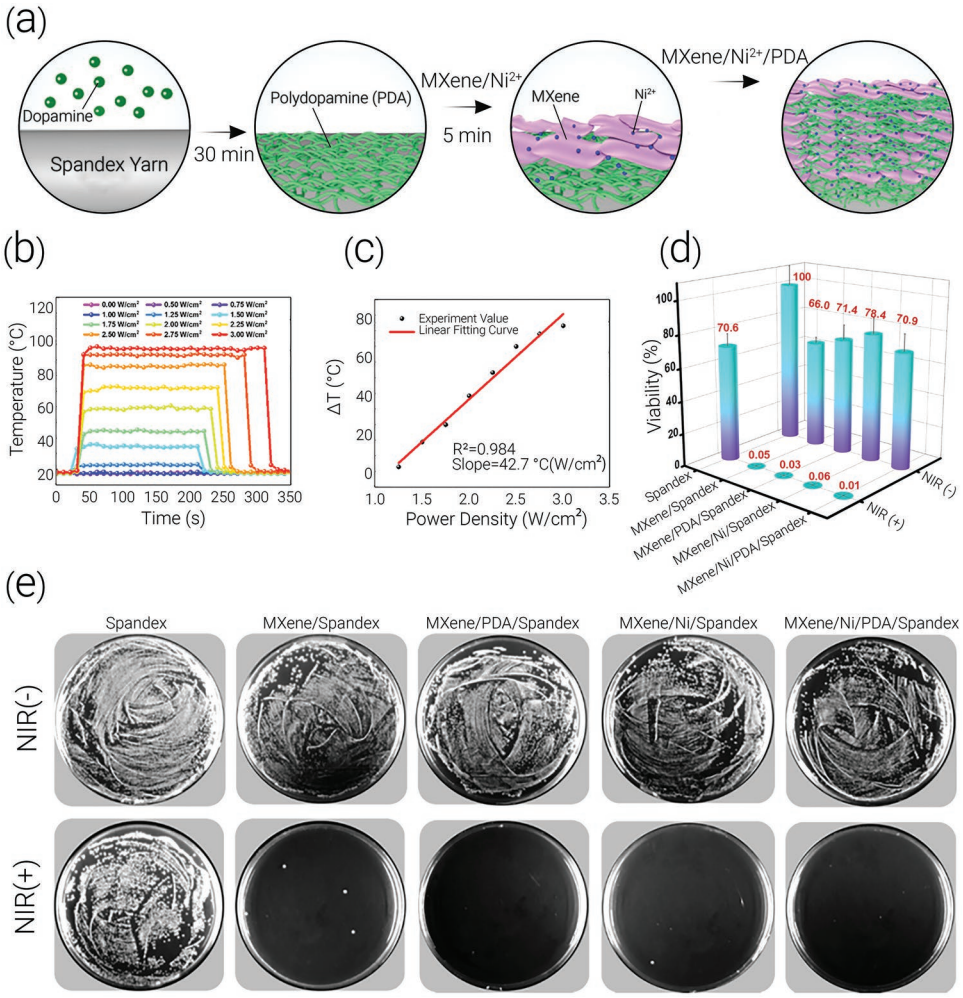

Figure 20. a) Description for preparation of conductive MPNi/Spandex composite coating. b) The time-dependent surface temperature of MPNi/Spandex composite coating upon irradiation by NIR with different intensities. c) A linear relationship between equilibrium temperature and NIR intensity. d,e) Viability of *E. coli* after exposure to different modified Spandex textiles in the presence and absence of NIR irradiation (Abbreviations: M = MXene, P = polydopamine, Ni = Ni^{2+} ions). Adapted with permission.[231] Copyright 2021, American Chemical Society.

compared to that of the corresponding MXenes while ROS generation by MAX phases is much less than MXenes. Therefore, not only the ROS content but also direct physicochemical interactions between the cells with MXenes have a great influence on the final cytotoxicity.[234]

In vitro cell-based assays are the common methods for evaluating the cytotoxicity of nanomaterials including MXenes. One of the main biomedical applications of MXenes is cancer therapy[237] which the cytotoxicity of MXenes has been well studied in most of the published papers in this scope. In treating the cancerous (A549 and A375) cells by $Ti_3C_2T_x$ MXenes, the cell viability was above 70% even at a high MXene concentration of 500 mg L^{-1}.[101] Similarly, the use of $Ti_3C_2T_x$ MXene for photothermal ablation of 4T1 cancer cells showed no cytotoxicity even at high $Ti_3C_2T_x$ concentrations (600 µg mL^{-1}) for 48 h exposure time.[238] Evaluating cytotoxicity of $Ti_3C_2T_x$ and their precursors on human fibroblasts and HeLa cells indicated toxicity for TiC and MAX phases at a concentration of 400 µg mL^{-1} whereas the cell viability for $Ti_3C_2T_x$ remained above 80%.[239] Zhang et al. reported no cytotoxicity on umbilical vein endothelial cells (HUVECs) after exposure to $Ti_3C_2T_x$ nanosheets at a concentration of 500 µg mL^{-1}.[240]

The cytotoxicity of MXenes depends on the cell type since there are several studies reporting the cytotoxic effects of MXenes. Exposure of the human mesenchymal stem cells (hMSCs) to $Ti_3C_2T_x$ nanosheets at concentrations > 50 µg mL^{-1} reduced the cell proliferation significantly while at lower concentrations no obvious toxicity was observed.[241] Similarly, evaluating the cytotoxicity of $Ti_3C_2T_x$ MXene to neural stem cells showed high toxicity at MXenes concentrations > 25 µg mL^{-1} through severe apoptosis and disturbing the cell membrane.[242]

Interestingly, it was shown that oxidation of V_2CT_x can turn it into a toxic material for cells.[243] In vitro cytotoxicity of delaminated V_2CT_x onto immortalized keratinocytes (HaCaT) and malignant melanoma (A375) human cell lines indicated that over time the V^{2+} and V^{3+} species are converted to V^{4+} and V^{5+} counterparts. After 48 h only around 50% cell viability was

reported for the concentrations above 50 μg mL^{-1}.[244] Oxidation of Ti-based MXenes showed similar results. Oxidation of $Ti_3C_2T_x$ into TiO_2 upon sonication or thermal treatments increased the cytotoxicity of the MXene with cell viability of <20% for cancerous cell lines at an MXene concentration of 500 μg mL^{-1}.[245]

7. Conclusions and Future Perspectives

MXenes are a fast-growing family of 2D materials and antibacterial applications have been one of the areas of their studies since 2016. MXenes combination of hydrophilic surfaces with negative surface charges (−30 to −50 mV) and the possibility of changing the surface charges to positive mV by surface functionalization, control of 2D flake sizes from ≈100 nm to a few μm have made them a candidate for interaction with bacterial and killing them. MXenes have tunable optical properties and many of them have extinction peaks in the UV–Vis–NIR region. The rich electronic properties of MXenes contribute to generation of different ROS types (including $O_2^{\bullet-}$, $^{\bullet}OH$, and $^1O_2$) which are effective species for killing bacteria. The sharp edges of ≈1-nm-thick MXene flakes combined with ROS have been described as the main mechanism for deactivating bacteria. Regarding the antibacterial mode of action of MXenes, more studies are needed along with a comparison with other 2D nanomaterials. For example, one appealing feature of MXenes is having a high metallic conductivity with a plethora of transition metals that might contribute to their antibacterial activities.

Additionally, by shining light in the NIR wavelength MXenes can be heated up due to the photothermal activity of MXenes, which can kill bacteria by increasing the temperature as well as accelerate the penetration of MXenes sharp edges into the bacteria membrane. Future studies should focus on the temperature needed to achieve the antibacterial photothermal therapy for various MXenes with different photothermal activity, and investigate the possibilities if the temperature does not reach this threshold.

The thickness of the 2D sheets of MXenes can be controlled which is unique in the 2D world, by changing the number of M-X atomic layers (n in $M_{n+1}X_nT_x$), for example, Nb_2CT_x and $Nb_4C_3T_x$. The thinner MXenes (e.g., Nb_2CT_x) showed higher effectiveness against both gram-positive and gram-negative bacteria (including *S. aureus, B. subtilis, VRE, S. agalactiae, E. faecalis, Sarcina, K. pneumoniae, P. aeruginosa, A. baumannii, S. typhi, E. coli, B. cepacia, E. cloacae, E. aerogenes, and P. mirabilis*) possibly due to the sharper edges. Also, changes in number of M-X atomic layers can control the optical properties, and with many of M_2XT_x and $M_3C_2T_x$ (n = 1 and 2) having extinction peaks in UV–Vis–NIR region while $M_4C_3T_x$ MXenes (n = 3) have almost no peaks in this region. As a result, Nb_2CT_x, $TiVCT_x$, and $Ti_3C_2T_x$ (n = 1 and 2) are used for the photothermal eradication of different bacteria. Despite the versatile transition metal used for preparing MXenes, only three MXene families (Ti, V, and Nb) have been studied. Development of a dataset including various MXenes composed of different transition metals is urgently needed to understand how antibacterial activities of MXenes are affected by transition metals.

The span of studied MXenes' antibacterial applications varies from the fabrication of wound dressing materials for facilitating the wound healing process to the production of sterilized water through MXene-based membrane processes and solar-driven water purification systems. Furthermore, the biocidal activities of MXene coatings by inhibiting microbial corrosion play an important role in metal protection. Additionally, similar to other 2D nanomaterials,[246] MXenes have the potential to be used for antibacterial food packaging.

As cleavage of DNA by $Ti_3C_2T_x$ nanosheets was proposed using fluorescence imaging and flow cytometry techniques, exploring interactions of the MXenes with the DNA molecules can be of interest. Note that the MXene has different characteristics from GO; for example, the functional groups at the surface terminations (T_x) of the MXene flakes (such as =O, −OH, and −F) provide the flakes with high hydrophilicity, high negative surface charge, and excellent electronic conductivity. Time-resolved fluorescence techniques can characterize the kinetics and thermodynamics of DNA-MXene interactions, including adsorption and desorption processes. To better understand the interactions at the molecular scale, MD simulation should be implemented. These studies may reveal new applications of MXenes in medical, biomedical, bioscience, biosensors, and biotechnology fields.

One of the problems of available MXenes for long-term applications is the gradual oxidation in air or by oxygen-dissolved in aqueous media. This issue affects the photothermal, photoelectronic, and biocidal properties of MXenes. Accordingly, new strategies for improving the stability of MXenes are in demand. At the same time, developing new MXenes with higher environmental stabilities is crucial.

Acknowledgements

F.S. and A.A.S. contributed equally to this work. F.S., Y.H., and C.L. acknowledge the support by the International Innovation Center for Forest Chemicals at Nanjing Forestry University, National Natural Science Foundation of China (22068006 and 61571239), and H.X. thanks the NSERC Canada support. M.R.S. thanks the Gdańsk University of Technology (DEC-1/2021/IDUB/I.1Pt grant under the Platinum Establishing Top-Class Research Teams). B.A. acknowledges funding from the U.S. National Science Foundation (grant no. CMMI-2134607).

Conflict of Interest

The authors declare no conflict of interest.

Keywords

2D carbides, antibacterial, MXenes, water purification, wound dressing

Received: October 31, 2022
Revised: December 11, 2022
Published online: January 5, 2023

[1] M. Zeng, M. Chen, D. Huang, S. Lei, X. Zhang, L. Wang, Z. Cheng, *Mater. Horiz.* **2021**, *8*, 758.

[2] W. Qian, S. Xu, X. Zhang, C. Li, W. Yang, C. R. Bowen, Y. Yang, *Nano-Micro Lett.* **2021**, *13*, 156.
[3] Z. Li, Y. Chen, T. Ma, Y. Jiang, J. Chen, H. Pan, W. Sun, *Adv. Energy Mater.* **2021**, *11*, 2101202.
[4] H. Xu, H. Shang, C. Wang, Y. Du, *Small* **2021**, *17*, 2005092.
[5] Y. Zhou, H. Yin, S. Ai, *Coord. Chem. Rev.* **2021**, *447*, 214156.
[6] A. Halim, K.-Y. Qu, X.-F. Zhang, N.-P. Huang, *ACS Biomater. Sci. Eng.* **2021**, *7*, 3503.
[7] Y. Zheng, X. Hong, J. Wang, L. Feng, T. Fan, R. Guo, H. Zhang, *Adv. Healthcare Mater.* **2021**, *10*, 2001743.
[8] Y. Wang, M. Qiu, M. Won, E. Jung, T. Fan, N. Xie, S.-G. Chi, H. Zhang, J. S. Kim, *Coord. Chem. Rev.* **2019**, *400*, 213041.
[9] B. Ma, A. Bianco, *Small* **2021**, *17*, 2102557.
[10] V. Yadav, S. Roy, P. Singh, Z. Khan, A. Jaiswal, *Small* **2019**, *15*, 1803706.
[11] M. Naguib, O. Mashtalir, J. Carle, V. Presser, J. Lu, L. Hultman, Y. Gogotsi, M. W. Barsoum, *ACS Nano* **2012**, *6*, 1322.
[12] M. Naguib, M. Kurtoglu, V. Presser, J. Lu, J. Niu, M. Heon, L. Hultman, Y. Gogotsi, M. W. Barsoum, *Adv. Mater.* **2011**, *23*, 4248.
[13] P. Urbankowski, B. Anasori, T. Makaryan, D. Er, S. Kota, P. L. Walsh, M. Zhao, V. B. Shenoy, M. W. Barsoum, Y. Gogotsi, *Nanoscale* **2016**, *8*, 11385.
[14] B. Anasori, M. R. Lukatskaya, Y. Gogotsi, *Nat. Rev. Mater.* **2017**, *2*, 16098.
[15] M. Tahir, A. Ali Khan, S. Tasleem, R. Mansoor, W. K. Fan, *Energy Fuels* **2021**, *35*, 10374.
[16] X. Wu, P. Ma, Y. Sun, F. Du, D. Song, G. Xu, *Electroanalysis* **2021**, *33*, 1827.
[17] A. A. Shamsabadi, A. P. Isfahani, S. K. Salestan, A. Rahimpour, B. Ghalei, E. Sivaniah, M. Soroush, *ACS Appl. Mater. Interfaces* **2019**, *12*, 3984.
[18] A. A. Shamsabadi, Z. Fakhraai, M. Soroush, *Mxenes and their Composites*, Elsevier, Amsterdam **2022**, pp 595.
[19] X. Lin, Z. Li, J. Qiu, Q. Wang, J. Wang, H. Zhang, T. Chen, *Biomater. Sci.* **2021**, *9*, 5437.
[20] H. Zhou, F. Wang, Y. Wang, C. Li, C. Shi, Y. Liu, Z. Ling, *RSC Adv.* **2021**, *11*, 5512.
[21] A. S. Zeraati, S. A. Mirkhani, P. Sun, M. Naguib, P. V. Braun, U. Sundararaj, *Nanoscale* **2021**, *13*, 3572.
[22] X. Jiang, S. Liu, W. Liang, S. Luo, Z. He, Y. Ge, H. Wang, R. Cao, F. Zhang, Q. Wen, *Laser Photonics Rev.* **2018**, *12*, 1700229.
[23] K. Fu, X. Liu, D. Yu, J. Luo, Z. Wang, J. C. Crittenden, *Environ. Sci. Technol.* **2020**, *54*, 16212.
[24] A. Lipatov, M. Alhabeb, H. Lu, S. Zhao, M. J. Loes, N. S. Vorobeva, Y. Dall'Agnese, Y. Gao, A. Gruverman, Y. Gogotsi, *Adv. Electron. Mater.* **2020**, *6*, 1901382.
[25] U. Amara, I. Hussain, M. Ahmad, K. Mahmood, K. Zhang, *Small* **2022**, 2205249.
[26] M. Wu, Q. Zhang, Y. Fang, C. Deng, F. Zhou, Y. Zhang, X. Wang, Y. Tang, Y. Wang, *J. Colloid Interface Sci.* **2021**, *586*, 20.
[27] V. Myndrul, E. Coy, N. Babayevska, V. Zahorodna, V. Balitskyi, I. Baginskiy, O. Gogotsi, M. Bechelany, M. T. Giardi, I. Iatsunskyi, *Biosens. Bioelectron.* **2022**, *207*, 114141.
[28] F. Mohajer, G. M. Ziarani, A. Badiei, S. Iravani, R. S. Varma. Advanced MXene-Based Micro- and Nanosystems for Targeted Drug Delivery in Cancer Therapy Micromachines [Online], **2022**.
[29] M. Wan, S. Song, X. Jiang, Z. Liu, Y. Luo, X. Gao, J. Liu, J. Shen, *ACS Appl. Nano Mater.* **2022**, *5*, 15583.
[30] N. Gao, J. Zhao, X. Zhu, J. Xu, G. Ling, P. Zhang, *ActaBiomater.* **2022**.
[31] R. Teixeira-Santos, M. Gomes, L. C. Gomes, F. J. Mergulhão, *iScience* **2021**, *24*, 102001.
[32] H. Ji, H. Sun, X. Qu, *Adv. Drug Del. Rev.* **2016**, *105*, 176.
[33] X. Zou, L. Zhang, Z. Wang, Y. Luo, *J. Am. Chem. Soc.* **2016**, *138*, 2064.
[34] M. D. Firouzjaei, A. A. Shamsabadi, M. Sharifian Gh, A. Rahimpour, M. Soroush, *Adv. Mater. Interfaces* **2018**, *5*, 1701365.
[35] A. Zirehpour, A. Rahimpour, A. Arabi Shamsabadi, M. Sharifian Gh, M. Soroush, *Environ. Sci. Technol.* **2017**, *51*, 5511.
[36] S. F. Seyedpour, A. Arabi Shamsabadi, S. Khoshhal Salestan, M. Dadashi Firouzjaei, M. Sharifian Gh, A. Rahimpour, F. Akbari Afkhami, M. R. Shirzad Kebria, M. A. Elliott, A. Tiraferri, *ACS Sustainable Chem. Eng.* **2020**, *8*, 7588.
[37] S. Chernousova, M. Epple, *Angew Chem Int Ed Engl* **2013**, *52*, 1636.
[38] A. Rahimpour, S. F. Seyedpour, S. Aghapour Aktij, M. Dadashi Firouzjaei, A. Zirehpour, A. Arabi Shamsabadi, S. Khoshhal Salestan, M. Jabbari, M. Soroush, *Environ. Sci. Technol.* **2018**, *52*, 5246.
[39] A. Raghunath, E. Perumal, *Int. J. Antimicrob. Agents* **2017**, *49*, 137.
[40] K. Usha, A. K. Nicholas, J. S. VanEpps*, *Curr. Pharm. Des.* **2018**, *24*, 896.
[41] Z. Ling, C. E. Ren, M.-Q. Zhao, J. Yang, J. M. Giammarco, J. Qiu, M. W. Barsoum, Y. Gogotsi, *Proc. Natl. Acad. Sci. USA* **2014**, *111*, 16676.
[42] Y. Dong, S. Chertopalov, K. Maleski, B. Anasori, L. Hu, S. Bhattacharya, A. M. Rao, Y. Gogotsi, V. N. Mochalin, R. Podila, *Adv. Mater.* **2018**, *30*, 1705714.
[43] L. Ding, Y. Wei, Y. Wang, H. Chen, J. Caro, H. Wang, *Angew. Chem., Int. Ed.* **2017**, *56*, 1825.
[44] R. P. Pandey, K. Rasool, V. E. Madhavan, B. Aïssa, Y. Gogotsi, K. A. Mahmoud, *J. Mater. Chem. A* **2018**, *6*, 3522.
[45] G. Liu, J. Shen, Q. Liu, G. Liu, J. Xiong, J. Yang, W. Jin, *J. Membr. Sci.* **2018**, *548*, 548.
[46] S. He, X. Sun, H. Zhang, C. Yuan, Y. Wei, J. Li, *Macromol. Rapid Commun.* **2021**, *42*, 2100324.
[47] K. Chen, N. Qiu, Q. Deng, M.-H. Kang, H. Yang, J.-U. Baek, Y.-H. Koh, S. Du, Q. Huang, H.-E. Kim, *ACS Biomater. Sci. Eng.* **2017**, *3*, 2293.
[48] H. Lin, Y. Chen, J. Shi, *Adv. Sci.* **2018**, *5*, 1800518.
[49] M. W. Barsoum, M. Radovic, *Annu. Rev. Mater. Res.* **2011**, *41*, 195.
[50] Z. M. Sun, *Int. Mater. Rev.* **2011**, *56*, 143.
[51] M. Sokol, V. Natu, S. Kota, M. W. Barsoum, *Trends in Chemistry* **2019**, *1*, 210.
[52] A. VahidMohammadi, J. Rosen, Y. Gogotsi, *Science* **2021**, *372*, eabf1581.
[53] S. Yang, P. Zhang, F. Wang, A. G. Ricciardulli, M. R. Lohe, P. W. Blom, X. Feng, *Angew. Chem.* **2018**, *130*, 15717.
[54] P. Urbankowski, B. Anasori, K. Hantanasirisakul, L. Yang, L. Zhang, B. Haines, S. J. May, S. J. Billinge, Y. Gogotsi, *Nanoscale* **2017**, *9*, 17722.
[55] J. Jeon, Y. Park, S. Choi, J. Lee, S. S. Lim, B. H. Lee, Y. J. Song, J. H. Cho, Y. H. Jang, S. Lee, *ACS Nano* **2018**, *12*, 338.
[56] Z. Lin, L. Cai, W. Lu, Y. Chai, *Small* **2017**, *13*, 1700051.
[57] Y. Gogotsi, *Nat. Mater.* **2015**, *14*, 1079.
[58] X. Xiao, P. Urbankowski, K. Hantanasirisakul, Y. Yang, S. Sasaki, L. Yang, C. Chen, H. Wang, L. Miao, S. H. Tolbert, *Adv. Funct. Mater.* **2019**, *29*, 1809001.
[59] F. Liu, A. Zhou, J. Chen, J. Jia, W. Zhou, L. Wang, Q. Hu, *Appl. Surf. Sci.* **2017**, *416*, 781.
[60] M. Ghidiu, M. R. Lukatskaya, M.-Q. Zhao, Y. Gogotsi, M. W. Barsoum, *Nature* **2014**, *516*, 78.
[61] X. Wang, C. Garnero, G. Rochard, D. Magne, S. Morisset, S. Hurand, P. Chartier, J. Rousseau, T. Cabioc'h, C. Coutanceau, V. Mauchamp, S. Célérier, *J. Mater. Chem. A* **2017**, *5*, 22012.
[62] J. Halim, M. R. Lukatskaya, K. M. Cook, J. Lu, C. R. Smith, L.-Å. Näslund, S. J. May, L. Hultman, Y. Gogotsi, P. Eklund, M. W. Barsoum, *Chem. Mater.* **2014**, *26*, 2374.

[63] T. Li, L. Yao, Q. Liu, J. Gu, R. Luo, J. Li, X. Yan, W. Wang, P. Liu, B. Chen, W. Zhang, W. Abbas, R. Naz, D. Zhang, *Angew. Chem., Int. Ed.* **2018**, *57*, 6115.
[64] J. Xuan, Z. Wang, Y. Chen, D. Liang, L. Cheng, X. Yang, Z. Liu, R. Ma, T. Sasaki, F. Geng, *Angew. Chem., Int. Ed.* **2016**, *55*, 14569.
[65] W. Sun, S. A. Shah, Y. Chen, Z. Tan, H. Gao, T. Habib, M. Radovic, M. J. Green, *J. Mater. Chem. A* **2017**, *5*, 21663.
[66] S.-Y. Pang, Y.-T. Wong, S. Yuan, Y. Liu, M.-K. Tsang, Z. Yang, H. Huang, W.-T. Wong, J. Hao, *J. Am. Chem. Soc.* **2019**, *141*, 9610.
[67] Y. Li, H. Shao, Z. Lin, J. Lu, L. Liu, B. Duployer, P. O. Å. Persson, P. Eklund, L. Hultman, M. Li, K. Chen, X.-H. Zha, S. Du, P. Rozier, Z. Chai, E. Raymundo-Piñero, P.-L. Taberna, P. Simon, Q. Huang, *Nat. Mater.* **2020**, *19*, 894.
[68] K. R. G. Lim, M. Shekhirev, B. C. Wyatt, B. Anasori, Y. Gogotsi, Z. W. Seh, *Nat., Synth.* **2022**, *1*, 601.
[69] O. Mashtalir, M. Naguib, V. N. Mochalin, Y. Dall'Agnese, M. Heon, M. W. Barsoum, Y. Gogotsi, *Nat. Commun.* **2013**, *4*, 1716.
[70] O. Mashtalir, M. R. Lukatskaya, M.-Q. Zhao, M. W. Barsoum, Y. Gogotsi, *Adv. Mater.* **2015**, *27*, 3501.
[71] M. Naguib, R. R. Unocic, B. L. Armstrong, J. Nanda, *Dalton Trans.* **2015**, *44*, 9353.
[72] P. Simon, *ACS Nano* **2017**, *11*, 2393.
[73] M. R. Lukatskaya, O. Mashtalir, C. E. Ren, Y. Dall'Agnese, P. Rozier, P. L. Taberna, M. Naguib, P. Simon, M. W. Barsoum, Y. Gogotsi, *Science* **2013**, *341*, 1502.
[74] C. Eames, M. S. Islam, *J. Am. Chem. Soc.* **2014**, *136*, 16270.
[75] A. Inman, V. Šedajová, K. Matthews, J. Gravlin, J. Busa, C. E. Shuck, A. VahidMohammadi, A. Bakandritsos, M. Shekhirev, M. Otyepka, Y. Gogotsi, *J. Mater. Res.* **2022**, *37*, 4006.
[76] Y. Xie, M. Naguib, V. N. Mochalin, M. W. Barsoum, Y. Gogotsi, X. Yu, K.-W. Nam, X.-Q. Yang, A. I. Kolesnikov, P. R. C. Kent, *J. Am. Chem. Soc.* **2014**, *136*, 6385.
[77] Y.-X. Yu, *J. Phys. Chem. C* **2016**, *120*, 5288.
[78] X. Ji, K. Xu, C. Chen, B. Zhang, Y. Ruan, J. Liu, L. Miao, J. Jiang, *Phys. Chem. Chem. Phys.* **2016**, *18*, 4460.
[79] M. Mariano, O. Mashtalir, F. Q. Antonio, W.-H. Ryu, B. Deng, F. Xia, Y. Gogotsi, A. D. Taylor, *Nanoscale* **2016**, *8*, 16371.
[80] A. Miranda, J. Halim, A. Lorke, M. W. Barsoum, *Mater. Res. Lett.* **2017**, *5*, 322.
[81] L. Lorencova, T. Bertok, E. Dosekova, A. Holazova, D. Paprckova, A. Vikartovska, V. Sasinkova, J. Filip, P. Kasak, M. Jerigova, D. Velic, K. A. Mahmoud, J. Tkac, *Electrochim. Acta* **2017**, *235*, 471.
[82] K. Rajavel, S. Shen, T. Ke, D. Lin, *2D Mater.* **2019**, *6*, 035040.
[83] R. P. Pandey, P. A. Rasheed, T. Gomez, K. Rasool, J. Ponraj, K. Prenger, M. Naguib, K. A. Mahmoud, *ACS Appl. Nano Mater.* **2020**, *3*, 11372.
[84] I. R. Shein, A. L. Ivanovskii, *Superlattices Microstruct.* **2012**, *52*, 147.
[85] Z. Bao, C. Lu, X. Cao, P. Zhang, L. Yang, H. Zhang, D. Sha, W. He, W. Zhang, L. Pan, Z. Sun, *Chin. Chem. Lett.* **2021**, *32*, 2648.
[86] Z. H. Fu, Q. F. Zhang, D. Legut, C. Si, T. C. Germann, T. Lookman, S. Y. Du, J. S. Francisco, R. F. Zhang, *Phys. Rev. B* **2016**, *94*, 104103.
[87] T. Hu, M. Hu, B. Gao, W. Li, X. Wang, *J. Phys. Chem. C* **2018**, *122*, 18501.
[88] J. L. Hart, K. Hantanasirisakul, A. C. Lang, B. Anasori, D. Pinto, Y. Pivak, J. T. van Omme, S. J. May, Y. Gogotsi, M. L. Taheri, *Nat. Commun.* **2019**, *10*, 522.
[89] O. Akhavan, E. Ghaderi, *ACS Nano* **2010**, *4*, 5731.
[90] O. Akhavan, E. Ghaderi, *Carbon* **2012**, *50*, 1853.
[91] K. Maleski, C. E. Shuck, A. T. Fafarman, Y. Gogotsi, *Adv. Opt. Mater.* **2021**, *9*, 2001563.
[92] K. Hantanasirisakul, Y. Gogotsi, *Adv. Mater.* **2018**, *30*, 1804779.
[93] H. Lin, S. Gao, C. Dai, Y. Chen, J. Shi, *J. Am. Chem. Soc.* **2017**, *139*, 16235.
[94] D. Xu, Z. Li, L. Li, J. Wang, *Adv. Funct. Mater.* **2020**, *30*, 2000712.
[95] R. Li, L. Zhang, L. Shi, P. Wang, *ACS Nano* **2017**, *11*, 3752.
[96] S. Hao, H. Han, Z. Yang, M. Chen, Y. Jiang, G. Lu, L. Dong, H. Wen, H. Li, J. Liu, L. Wu, Z. Wang, F. Wang, *Nano-Micro Lett.* **2022**, *14*, 178.
[97] T.-K. Nguyen, H. T. T. Duong, R. Selvanayagam, C. Boyer, N. Barraud, *Sci. Rep.* **2015**, *5*, 18385.
[98] Q. Zhao, J. Wang, C. Yin, P. Zhang, J. Zhang, M. Shi, K. Shen, Y. Xiao, Y. Zhao, X. Yang, Y. Zhang, *Nano Lett.* **2019**, *19*, 5904.
[99] J. M. A. Blair, M. A. Webber, A. J. Baylay, D. O. Ogbolu, L. J. V. Piddock, *Nat. Rev. Microbiol.* **2015**, *13*, 42.
[100] G. Liu, J. Zou, Q. Tang, X. Yang, Y. Zhang, Q. Zhang, W. Huang, P. Chen, J. Shao, X. Dong, *ACS Appl Mater Interfaces* **2017**, *9*, 40077.
[101] A. Jastrzębska, A. Szuplewska, T. Wojciechowski, M. Chudy, W. Ziemkowska, L. Chlubny, A. Rozmysłowska, A. Olszyna, *J. Hazard. Mater.* **2017**, *339*, 1.
[102] F. Wu, H. Zheng, W. Wang, Q. Wu, Q. Zhang, J. Guo, B. Pu, X. Shi, J. Li, X. Chen, *Sci. China Mater.* **2021**, *64*, 748.
[103] X. Wang, M. Yao, L. Ma, P. Yu, T. Lu, L. Zhang, X. Yuan, Y. Zhang, J. Ye, *Adv. Healthcare Mater.* **2021**, 2100392.
[104] J. K. El-Demellawi, S. Lopatin, J. Yin, O. F. Mohammed, H. N. Alshareef, *ACS Nano* **2018**, *12*, 8485.
[105] W. Zhai, Y. Cao, Y. Li, M. Zheng, Z. Wang, *J. Mater. Sci.* **2022**, *1*.
[106] J.-W. Xu, K. Yao, Z.-K. Xu, *Nanoscale* **2019**, *11*, 8680.
[107] Y. Chen, Y. Gao, Y. Chen, L. Liu, A. Mo, Q. Peng, *J. Controlled Release* **2020**, *328*, 251.
[108] S. Y. Kim, C. Park, H.-J. Jang, B.-o. Kim, H.-W. Bae, I.-Y. Chung, E. S. Kim, Y.-H. Cho, *J Microbiol* **2019**, *57*, 203.
[109] Á. Mourenza, J. A. Gil, L. M. Mateos, M. Letek, *Antioxidants* **2020**, *9*.
[110] Y. Zhang, A. Clapp, *Sensors* **2011**, *11*, 11036.
[111] R. M. McDaniel, M. S. Carey, O. R. Wilson, M. W. Barsoum, A. J. D. Magenau, *Chem. Mater.* **2021**, *33*, 1648.
[112] J. T. Lee, B. C. Wyatt, G. A. Davis Jr., A. N. Masterson, A. L. Pagan, A. Shah, B. Anasori, R. Sardar, *ACS Nano* **2021**, *15*, 19600.
[113] P. Wick, P. Manser, L. K. Limbach, U. Dettlaff-Weglikowska, F. Krumeich, S. Roth, W. J. Stark, A. Bruinink, *Toxicol. Lett.* **2007**, *168*, 121.
[114] X. Wang, X. Liu, H. Han, *Colloids Surf., B* **2013**, *103*, 136.
[115] S. Liu, T. H. Zeng, M. Hofmann, E. Burcombe, J. Wei, R. Jiang, J. Kong, Y. Chen, *ACS Nano* **2011**, *5*, 6971.
[116] K. Rasool, K. A. Mahmoud, 2D metal carbide antimicrobial membrane and antimicrobial agent. Google Patents: **2019**.
[117] K. Rasool, R. P. Pandey, P. A. Rasheed, G. R. Berdiyorov, K. A. Mahmoud, *2D Metal Carbides and Nitrides (MXenes)*, Springer, **2019**, pp 417.
[118] K. A. S. Usman, S. Qin, L. C. Henderson, J. Zhang, D. Y. Hegh, J. M. Razal, *Mater. Horiz.* **2021**, *8*, 2886.
[119] B. Akuzum, K. Maleski, B. Anasori, P. Lelyukh, N. J. Alvarez, E. C. Kumbur, Y. Gogotsi, *ACS Nano* **2018**, *12*, 2685.
[120] S. Shen, T. Ke, K. Rajavel, K. Yang, D. Lin, *Small* **2020**, *16*, 2002433.
[121] K. Hantanasirisakul, M.-Q. Zhao, P. Urbankowski, J. Halim, B. Anasori, S. Kota, C. E. Ren, M. W. Barsoum, Y. Gogotsi, *Adv. Electron. Mater.* **2016**, *2*, 1600050.
[122] A. D. Dillon, M. J. Ghidiu, A. L. Krick, J. Griggs, S. J. May, Y. Gogotsi, M. W. Barsoum, A. T. Fafarman, *Adv. Funct. Mater.* **2016**, *26*, 4162.
[123] X. Zhan, C. Si, J. Zhou, Z. Sun, *Nanoscale Horiz.* **2020**, *5*, 235.
[124] Y. Zeng, W. Wu, *Nanoscale Horiz.* **2021**, *6*, 893.
[125] C. J. Zhang, S. Pinilla, N. McEvoy, C. P. Cullen, B. Anasori, E. Long, S.-H. Park, A. Seral-Ascaso, A. Shmeliov, D. Krishnan, C. Morant, X. Liu, G. S. Duesberg, Y. Gogotsi, V. Nicolosi, *Chem. Mater.* **2017**, *29*, 4848.
[126] O. Mashtalir, K. M. Cook, V. N. Mochalin, M. Crowe, M. W. Barsoum, Y. Gogotsi, *J. Mater. Chem. A* **2014**, *2*, 14334.
[127] S. Huang, V. N. Mochalin, *Inorg. Chem.* **2019**, *58*, 1958.
[128] M. Alhabeb, K. Maleski, B. Anasori, P. Lelyukh, L. Clark, S. Sin, Y. Gogotsi, *Chem. Mater.* **2017**, *29*, 7633.

[129] X. Zhao, A. Vashisth, E. Prehn, W. Sun, S. A. Shah, T. Habib, Y. Chen, Z. Tan, J. L. Lutkenhaus, M. Radovic, M. J. Green, *Matter* **2019**, *1*, 513.
[130] M. Naguib, O. Mashtalir, M. R. Lukatskaya, B. Dyatkin, C. Zhang, V. Presser, Y. Gogotsi, M. W. Barsoum, *Chem. Commun.* **2014**, *50*, 7420.
[131] K. Rasool, K. A. Mahmoud, D. J. Johnson, M. Helal, G. R. Berdiyorov, Y. Gogotsi, *Sci. Rep.* **2017**, *7*, 1.
[132] F. Perreault, A. F. De Faria, S. Nejati, M. Elimelech, *ACS Nano* **2015**, *9*, 7226.
[133] S. F. Seyedpour, A. Rahimpour, A. A. Shamsabadi, M. Soroush, *Chem. Eng. Res. Des.* **2018**, *139*, 321.
[134] A. Arabi Shamsabadi, M. Sharifian Gh, B. Anasori, M. Soroush, *ACS Sustainable Chem. Eng.* **2018**, *6*, 16586.
[135] S. Huo, Y. Gao, L. Fang, Z. Jiang, Q. Xie, Q. Meng, G. Fei, S. Ding, *Appl. Surf. Sci.* **2021**, *551*, 149444.
[136] M. D. Firouzjaei, A. A. Shamsabadi, S. A. Aktij, S. F. Seyedpour, M. Sharifian Gh, A. Rahimpour, M. R. Esfahani, M. Ulbricht, M. Soroush, *ACS Appl. Mater. Interfaces* **2018**, *10*, 42967.
[137] H. Riazi, M. Anayee, K. Hantanasirisakul, A. A. Shamsabadi, B. Anasori, Y. Gogotsi, M. Soroush, *Adv. Mater. Interfaces* **2020**, *7*, 1902008.
[138] A. Rozmysłowska-Wojciechowska, J. Mitrzak, A. Szuplewska, M. Chudy, J. Woźniak, M. Petrus, T. Wojciechowski, A. S. Vasilchenko, A. M. Jastrzębska, *Materials* **2020**, *13*, 2347.
[139] M. Mansoorianfar, K. Shahin, A. Hojjati–Najafabadi, R. Pei, *Chemosphere* **2021**, *290*, 133383.
[140] O.-S. Lee, M. E. Madjet, K. A. Mahmoud, *Nano Lett.* **2021**, *21*, 8510.
[141] K. Rasool, M. Helal, A. Ali, C. E. Ren, Y. Gogotsi, K. A. Mahmoud, *ACS Nano* **2016**, *10*, 3674.
[142] L. Wu, L. Zeng, X. Jiang, *J. Am. Chem. Soc.* **2015**, *137*, 10052.
[143] S. Romero-Vargas Castrillón, F. o. Perreault, A. F. De Faria, M. Elimelech, *Environ. Sci. Technol. Lett.* **2015**, *2*, 112.
[144] X. Santos, M. Álvarez, D. Videira-Quintela, A. Mediero, J. Rodríguez, F. Guillén, J. Pozuelo, O. Martín, *Membranes* **2022**, *12*, 1146.
[145] R. Godlewska, K. Wiśniewska, Z. Pietras, E. K. Jagusztyn-Krynicka, *FEMS Microbiol. Lett.* **2009**, *298*, 1.
[146] A. Popescu, R. Doyle, *Biotech. Histochem.* **1996**, *71*, 145.
[147] L. Wang, Y. Li, L. Zhao, Z. Qi, J. Gou, S. Zhang, J. Z. Zhang, *Nanoscale* **2020**, *12*, 19516.
[148] D.-Y. Zhang, H. Liu, M. R. Younis, S. Lei, Y. Chen, P. Huang, J. Lin, *J. Nanobiotechnol.* **2022**, *20*, 53.
[149] H. Wang, X. Liu, X. Yan, J. Fan, D. Li, J. Ren, X. Qu, *Chem. Sci.* **2022**, *13*, 6704.
[150] G. Li, X. Zhong, X. Wang, F. Gong, H. Lei, Y. Zhou, C. Li, Z. Xiao, G. Ren, L. Zhang, Z. Dong, Z. Liu, L. Cheng, *Bioact Mater* **2022**, *8*, 409.
[151] B. Geng, S. Xu, L. Shen, F. Fang, W. Shi, D. Pan, *Carbon* **2021**, *179*, 493.
[152] M. Zhang, D. Yang, C. Dong, H. Huang, G. Feng, Q. Chen, Y. Zheng, H. Tang, Y. Chen, X. Jing, *ACS Nano* **2022**, *16*, 9938.
[153] K. Krumova, G. Cosa, **2016**.
[154] S. González-Poggini, A. Rosenkranz, M. Colet-Lagrille, *Processes* **2021**, *9*, 2160.
[155] J. Zhao, Z. Wang, J. C. White, B. Xing, *Environ. Sci. Technol.* **2014**, *48*, 9995.
[156] H. Pieper, S. Chercheja, S. Eigler, C. E. Halbig, M. R. Filipovic, A. Mokhir, *Angew. Chem., Int. Ed.* **2016**, *55*, 405.
[157] M. Khazaei, A. Ranjbar, M. Arai, T. Sasaki, S. Yunoki, *J. Mater. Chem. C* **2017**, *5*, 2488.
[158] S. Ye, M. Yan, X. Tan, J. Liang, G. Zeng, H. Wu, B. Song, C. Zhou, Y. Yang, H. Wang, *Appl. Catal., B* **2019**, *250*, 78.
[159] M. Rosales, A. Garcia, V. M. Fuenzalida, R. Espinoza-González, G. Song, B. Wang, J. Yu, F. Gracia, A. Rosenkranz, *Appl. Mater. Today* **2020**, *20*, 100769.
[160] Y. Bai, K. Zhou, N. Srikanth, J. H. L. Pang, X. He, R. Wang, *RSC Adv.* **2016**, *6*, 35731.
[161] H. Lin, X. Wang, L. Yu, Y. Chen, J. Shi, *Nano Lett.* **2017**, *17*, 384.
[162] G. Cebrián, S. Condón, P. Mañas, *Foods* **2017**, *6*, 107.
[163] X. Yu, X. Cai, H. Cui, S.-W. Lee, X.-F. Yu, B. Liu, *Nanoscale* **2017**, *9*, 17859.
[164] B. Kramer, J. Thielmann, *J Microbiol Methods* **2016**, *123*, 24.
[165] I. Leguérinel, I. Spegagne, O. Couvert, L. Coroller, P. Mafart, *Int. J. Food Microbiol.* **2007**, *116*, 88.
[166] A. Schön, E. Freire, *Anal. Biochem.* **2021**, *626*, 114240.
[167] D. Wu, R. Zhao, Y. Chen, Y. Wang, J. Li, Y. Fan, *Phys. Chem. Chem. Phys.* **2021**, *23*, 3341.
[168] X. Yi, H. Gao, *Nanoscale* **2015**, *7*, 5457.
[169] K. Yang, Y.-Q. Ma, *Nat. Nanotechnol.* **2010**, *5*, 579.
[170] C. J. Jameson, P. Oroskar, B. Song, H. Yuan, S. Murad, *Biomimetic Lipid Membranes: Fundamentals, Applications, and Commercialization*, Springer, Berlin **2019**, pp 109.
[171] V. K. Gangupomu, F. M. Capaldi, *J. Nanomater.* **2011**, *2011*, 830436.
[172] P. Raczyński, K. Górny, P. Bełdowski, S. Yuvan, Z. Dendzik, *J. Phys. Chem. B* **2020**, *124*, 6592.
[173] W. Hu, C. Peng, W. Luo, M. Lv, X. Li, D. Li, Q. Huang, C. Fan, *ACS Nano* **2010**, *4*, 4317.
[174] F. Fu, L. Li, L. Liu, J. Cai, Y. Zhang, J. Zhou, L. Zhang, *ACS Appl. Mater. Interfaces* **2015**, *7*, 2597.
[175] T. Ozulumba, G. Ingavle, Y. Gogotsi, S. Sandeman, *Biomater. Sci.* **2021**, *9*, 1805.
[176] A. M. Jastrzębska, E. Karwowska, T. Wojciechowski, W. Ziemkowska, A. Rozmysłowska, L. Chlubny, A. Olszyna, *J. Mater. Eng. Perform.* **2019**, *28*, 1272.
[177] A. Jastrzebska, E. Karwowska, D. Basiak, A. Zawada, W. Ziemkowska, T. Wojciechowski, D. Jakubowska, A. Olszyna, *Int J Electrochem Sci* **2017**, *12*, 2159.
[178] Q. He, H. Hu, J. Han, Z. Zhao, *Mater. Lett.* **2022**, *308*, 131100.
[179] W. Zheng, P. Zhang, W. Tian, Y. Wang, Y. Zhang, J. Chen, Z. Sun, *Mater. Lett.* **2017**, *209*, 122.
[180] C. Peng, X. Yang, Y. Li, H. Yu, H. Wang, F. Peng, *ACS Appl Mater Interfaces* **2016**, *8*, 6051.
[181] F. Wang, C. Yang, M. Duan, Y. Tang, J. Zhu, *Biosens. Bioelectron.* **2015**, *74*, 1022.
[182] H. Zhang, H. Dong, X. Zhang, Y. Xu, J. Fransaer, *Electrochim. Acta* **2016**, *202*, 24.
[183] Q. Xue, Z. Pei, Y. Huang, M. Zhu, Z. Tang, H. Li, Y. Huang, N. Li, H. Zhang, C. Zhi, *J. Mater. Chem. A* **2017**, *5*, 20818.
[184] R. B. Rakhi, B. Ahmed, D. Anjum, H. N. Alshareef, *ACS Appl Mater Interfaces* **2016**, *8*, 18806.
[185] X. Guo, X. Xie, S. Choi, Y. Zhao, H. Liu, C. Wang, S. Chang, G. Wang, *J. Mater. Chem. A* **2017**, *5*, 12445.
[186] Y. Gao, L. Wang, A. Zhou, Z. Li, J. Chen, H. Bala, Q. Hu, X. Cao, *Mater. Lett.* **2015**, *150*, 62.
[187] F. Xia, J. Lao, R. Yu, X. Sang, J. Luo, Y. Li, J. Wu, *Nanoscale* **2019**, *11*, 23330.
[188] K. Rajavel, S. Shen, T. Ke, D. Lin, *Appl. Surf. Sci.* **2021**, *538*, 148083.
[189] X. Zhu, Y. Zhu, K. Jia, B. S. Abraha, Y. Li, W. Peng, F. Zhang, X. Fan, L. Zhang, *Nanoscale* **2020**, *12*, 19129.
[190] A. Rozmysłowska-Wojciechowska, E. Karwowska, S. Poźniak, T. Wojciechowski, L. Chlubny, A. Olszyna, W. Ziemkowska, A. M. Jastrzębska, *RSC Adv.* **2019**, *9*, 4092.
[191] H. Feng, W. Wang, M. Zhang, S. Zhu, Q. Wang, J. Liu, S. Chen, *Appl. Catal., B* **2020**, *266*, 118609.
[192] W. Wang, H. Feng, J. Liu, M. Zhang, S. Liu, C. Feng, S. Chen, *Chem. Eng. J.* **2020**, *386*, 124116.
[193] Z. Yang, X. Hao, S. Chen, Z. Ma, W. Wang, C. Wang, L. Yue, H. Sun, Q. Shao, V. Murugadoss, Z. Guo, *J. Colloid Interface Sci.* **2019**, *533*, 13.

[194] K. Zheng, S. Li, L. Jing, P. Y. Chen, J. Xie, *Adv. Healthcare Mater.* **2020**, *9*, 2001007.
[195] Y. Liu, Y. Tian, Q. Han, J. Yin, J. Zhang, Y. Yu, W. Yang, Y. Deng, *Chem. Eng. J.* **2021**, *410*, 128209.
[196] F. Alimohammadi, M. Sharifian Gh, N. H. Attanayake, A. C. Thenuwara, Y. Gogotsi, B. Anasori, D. R. Strongin, *Langmuir* **2018**, *34*, 7192.
[197] X. Yang, J. Li, T. Liang, C. Ma, Y. Zhang, H. Chen, N. Hanagata, H. Su, M. Xu, *Nanoscale* **2014**, *6*, 10126.
[198] C. Liu, D. Kong, P.-C. Hsu, H. Yuan, H.-W. Lee, Y. Liu, H. Wang, S. Wang, K. Yan, D. Lin, P. A. Maraccini, K. M. Parker, A. B. Boehm, Y. Cui, *Nat. Nanotechnol.* **2016**, *11*, 1098.
[199] Y. Wu, W. Zheng, Y. Xiao, B. Du, X. Zhang, M. Wen, C. Lai, Y. Huang, L. Sheng, *Polymers* **2021**, *13*, 3748.
[200] E. A. Kamoun, E.-R. S. Kenawy, X. Chen, *J Adv Res* **2017**, *8*, 217.
[201] Y. Yao, A. Zhang, C. Yuan, X. Chen, Y. Liu, *Biomater. Sci.* **2021**, *9*, 4523.
[202] Y. Zhong, F. Seidi, C. Li, Z. Wan, Y. Jin, J. Song, H. Xiao, *Biomacromolecules* **2021**, *22*, 1654.
[203] Y. Zhong, H. Xiao, F. Seidi, Y. Jin, *Biomacromolecules* **2020**, *21*, 2983.
[204] Y. Zhong, F. Seidi, Y. Wang, L. Zheng, Y. Jin, H. Xiao, *Carbohydr. Polym.* **2022**, 120103.
[205] B. Azimi, H. Maleki, L. Zavagna, J. G. De la Ossa, S. Linari, A. Lazzeri, S. Danti, *J Funct Biomater* **2020**, *11*, 62.
[206] L. Mao, S. Hu, Y. Gao, L. Wang, W. Zhao, L. Fu, H. Cheng, L. Xia, S. Xie, W. Ye, *Adv. Healthcare Mater.* **2020**, *9*, 2000872.
[207] A. F. de Faria, F. Perreault, E. Shaulsky, L. H. Arias Chavez, M. Elimelech, *ACS Appl. Mater. Interfaces* **2015**, *7*, 12751.
[208] A. Rozmysłowska-Wojciechowska, E. Karwowska, M. Gloc, J. Woźniak, M. Petrus, B. Przybyszewski, T. Wojciechowski, A. M. Jastrzębska, *Materials* **2020**, *13*, 4587.
[209] L. Zhou, H. Zheng, Z. Liu, S. Wang, Z. Liu, F. Chen, H. Zhang, J. Kong, F. Zhou, Q. Zhang, *ACS Nano* **2021**, *15*, 2468.
[210] J. Yin, Q. Han, J. Zhang, Y. Liu, X. Gan, K. Xie, L. Xie, Y. Deng, *ACS Appl Mater Interfaces* **2020**, *12*, 45891.
[211] J. Chen, Y. Liu, G. Cheng, J. Guo, S. Du, J. Qiu, C. Wang, C. Li, X. Yang, T. Chen, Z. Chen, *Small* **2022**, *18*.
[212] S. Zhang, J. Ye, X. Liu, Y. Wang, C. Li, J. Fang, B. Chang, Y. Qi, Y. Li, G. Ning, *J. Colloid Interface Sci.* **2021**, *599*, 390.
[213] C. Yang, Y. Luo, H. Lin, M. Ge, J. Shi, X. Zhang, *ACS Nano* **2021**, *15*, 1086.
[214] K. A. Mahmoud, B. Mansoor, A. Mansour, M. Khraisheh, *Desalination* **2015**, *356*, 208.
[215] J. Zhu, J. Wang, J. Hou, Y. Zhang, J. Liu, B. Van der Bruggen, *J. Mater. Chem. A* **2017**, *5*, 6776.
[216] J. Zhu, J. Hou, Y. Zhang, M. Tian, T. He, J. Liu, V. Chen, *J. Membr. Sci.* **2018**, *550*, 173.
[217] Y. Sun, M. Yang, F. Yu, J. Chen, J. Ma, *Progress in Chemistry* **2015**, *27*, 1133.
[218] Y. Feng, H. Wang, J. Xu, X. Du, X. Cheng, Z. Du, H. Wang, *J. Hazard. Mater.* **2021**, *416*, 125777.
[219] P. Tao, G. Ni, C. Song, W. Shang, J. Wu, J. Zhu, G. Chen, T. Deng, *Nat. Energy* **2018**, *3*, 1031.
[220] C. Chen, Y. Kuang, L. Hu, *Joule* **2019**, *3*, 683.
[221] M. Gao, L. Zhu, C. K. Peh, G. W. Ho, *Energy Environ. Sci.* **2019**, *12*, 841.
[222] G. Ni, G. Li, S. V. Boriskina, H. Li, W. Yang, T. Zhang, G. Chen, *Nat. Energy* **2016**, *1*, 16126.
[223] M. Zhu, Y. Li, F. Chen, X. Zhu, J. Dai, Y. Li, Z. Yang, X. Yan, J. Song, Y. Wang, *Adv. Energy Mater.* **2018**, *8*, 1701028.
[224] C. Chen, L. Zhou, J. Yu, Y. Wang, S. Nie, S. Zhu, J. Zhu, *Nano Energy* **2018**, *51*, 451.
[225] J. Zhao, Y. Yang, C. Yang, Y. Tian, Y. Han, J. Liu, X. Yin, W. Que, *J. Mater. Chem. A* **2018**, *6*, 16196.
[226] X. Zhao, X.-J. Zha, J.-H. Pu, L. Bai, R.-Y. Bao, Z.-Y. Liu, M.-B. Yang, W. Yang, *J. Mater. Chem. A* **2019**, *7*, 10446.
[227] X.-J. Zha, X. Zhao, J.-H. Pu, L.-S. Tang, K. Ke, R.-Y. Bao, L. Bai, Z.-Y. Liu, M.-B. Yang, W. Yang, *ACS Appl Mater Interfaces* **2019**, *11*, 36589.
[228] H. Liu, Y. Liu, L. Wang, X. Qin, J. Yu, *Carbon* **2021**, *177*, 199.
[229] Y. Nie, J. Huang, S. Ma, Z. Li, Y. Shi, X. Yang, X. Fang, J. Zeng, P. Bi, J. Qi, S. Wang, Y. Xia, T. Jiao, D. Li, M. Cao, *Appl. Surf. Sci.* **2020**, *527*, 146915.
[230] W. P. Iverson, *Adv. Appl. Microbiol.* **1987**, *32*, 1.
[231] M. Gong, L. Yue, J. Kong, X. Lin, L. Zhang, J. Wang, D. Wang, *ACS Appl Mater Interfaces* **2021**, *13*, 9053.
[232] M. Ema, M. Gamo, K. Honda, *Regul. Toxicol. Pharm.* **2017**, *85*, 7.
[233] R. Das, B. F. Leo, F. Murphy, *Nanoscale Res. Lett.* **2018**, *13*, 183.
[234] G. P. Lim, C. F. Soon, N. L. Ma, M. Morsin, N. Nayan, M. K. Ahmad, K. S. Tee, *Environ. Res.* **2021**, *201*, 111592.
[235] G. A. Naikoo, F. Arshad, M. Almas, I. U. Hassan, M. Z. Pedram, A. A. A. Aljabali, V. Mishra, A. Serrano-Aroca, M. Birkett, N. B. Charbe, R. Goyal, P. Negi, M. El-Tanani, M. M. Tambuwala, *Chem Biol Interact* **2022**, *365*, 110081.
[236] J. Wu, Y. Yu, G. Su, *Nanomaterials* **2022**, *12*, 828.
[237] K. Huang, Z. Li, J. Lin, G. Han, P. Huang, *Chem. Soc. Rev.* **2018**, *47*, 6889.
[238] X. Han, J. Huang, H. Lin, Z. Wang, P. Li, Y. Chen, *Adv. Healthcare Mater.* **2018**, *7*, 1701394.
[239] B. Scheibe, J. K. Wychowaniec, M. Scheibe, B. Peplinska, M. Jarek, G. Nowaczyk, L. Przysiecka, *ACS Biomater. Sci. Eng.* **2019**, *5*, 6557.
[240] D. Zhang, W. Zheng, X. Li, A. Li, N. Ye, L. Zhang, Y. Liu, X. Liu, R. Zhang, M. Wang, J. Cheng, H. Yang, M. Gong, *Carbon* **2021**, *178*, 810.
[241] J.-H. Jang, E.-J. Lee, *Materials* **2021**, *14*, 4453.
[242] W. Wu, H. Ge, L. Zhang, X. Lei, Y. Yang, Y. Fu, H. Feng, *Chem. Res. Toxicol.* **2020**, *33*, 2953.
[243] A. Szuplewska, A. Rozmyslowska-Wojciechowska, S. Pozniak, T. Wojciechowski, M. Birowska, M. Popielski, M. Chudy, W. Ziemkowska, L. Chlubny, D. Moszczynska, A. Olszyna, J. A. Majewski, A. M. Jastrzebska, *J. Nanobiotechnol.* **2019**, *17*, 114.
[244] A. M. Jastrzebska, B. Scheibe, A. Szuplewska, A. Rozmyslowska-Wojciechowska, M. Chudy, C. Aparicio, M. Scheibe, I. Janica, A. Ciesielski, M. Otyepka, M. W. Barsoum, *Mater. Sci. Eng. C-Mater. Biolog. Appl.* **2021**, *119*, 111431.
[245] A. M. Jastrzebska, A. Szuplewska, A. Rozmyslowska-Wojciechowska, M. Chudy, A. Olszyna, M. Birowska, M. Popielski, J. A. Majewski, B. Scheibe, V. Natu, M. W. Barsoum, *2D Mater.* **2020**, *7*, 025018.
[246] Y. Yu, J. Zheng, J. Li, L. Lu, J. Yan, L. Zhang, L. Wang, *Trends Food Sci. Technol.* **2021**, *110*, 443.

Farzad Seidi obtained his Ph.D. in organic and polymer chemistry at Sharif University of Technology in Iran in 2011. He carried out postdoctoral research from 2016 to 2019 in Thailand at the Vidyasirimedhi Institute of Science and Technology (VISTEC) with Prof. Daniel Crespy. Currently, he is an associate professor at Nanjing Forestry University in China. He has published over 170 peer-reviewed articles. His main expertise is polymer/colloid chemistry and design of functional materials for biomedical and industrial applications.

Ahmad Arabi Shamsabadi received his Ph.D. (Chemical Engineering) from Drexel University, U.S.A. After graduating from Drexel University, he joined the University of Pennsylvania as a Vagelos Institute for Energy Science and Technology (VIEST) postdoctoral fellow. Currently, he is an R&D senior scientist-polymer chemistry at Pall Corporation, New York. His research interests are in polymer membranes, gas separation, ion separation, water treatment, polymer thin-films and composites, and polymer chemistry. He has published >70 journal articles.

Mostafa Dadashi Firouzjaei, Ph.D., is an Assistant Research Professional at the University of Alabama. Mostafa's professional background includes time as a doctoral student and a post-doctoral research associate in the Civil Engineering department at the University of Alabama. He holds a master's degree in Materials Engineering and Environmental Engineering. Mostafa received a BSc in Materials Science and Engineering in 2011. His study's main areas are the selection, characterization, and development of novel materials for water/wastewater treatment and microbiological disinfection. Since 2015, Mostafa began researching and developing methods for synthesizing novel antifouling and anti-biofouling polymeric membranes for sustainable water recovery.

Mark Elliott, Ph.D., is an Associate Professor of environmental engineering at the University of Alabama. His research focuses primarily on water and wastewater challenges in low-resource settings, wastewater management in the rural southeastern US, and membrane-based treatment of water and wastewater.

Mohammad Reza Saeb works as University Prof. at the Department of Chemistry, Gdańsk University of Technology, Poland. He authored/co-authored >450 papers in high-ranked/indexed journals on exploration and explanation of association between microstructure, properties, and performance of nanomaterials, biomaterials, polymer blends, and polymer nanocomposites. He conceptualized and introduced *Cure Index* and *Flame Retardancy Index* for classification of polymer nanocomposites. He also developed several nanomaterials and biomaterials, along with hybrid nanocomposites for sustainable development of biomedical applications. He is currently working on management of waste polymers (obtained as PI ≈1.1 M€ in 2022 from Gdańsk University of Technology, namely PLATINUM project).

Huining Xiao obtained his Ph.D. in Chemical Eng. at McMaster University in Canada in 1995. Before joining the University of New Brunswick (UNB) Canada in 2001, he was a Lecturer at the University of Manchester in the UK from 1996 to 2001. Currently, he is a Professor in Chemical Eng. at UNB. His research interests focus on smart polymers and nanoparticles for functional-modified cellulose and green-based materials for the applications associated with personal protection equipment, barrier-enhanced packaging materials, the controlled release of drugs/agrochemicals, and water/soil remediation.

Babak Anasori is an assistant professor at the Purdue School of Engineering and Technology, Indiana University–Purdue University Indianapolis. He received his Ph.D. in materials science and engineering from Drexel University in 2014. He is one of the inventors of ordered double-transition metal MXenes and high-entropy MXenes. He has co-authored >150 journal papers and co-edited the first book on MXenes in 2019. He is among the *Web of Science* Highly Cited Researchers from 2019 to 2022. His lab works on the synthesis and characterizations of novel MXenes and their composites, mechanical, and electrocatalysis properties.